which is one of the fusion partners of *MLL*, as a novel fusion partner of the *AML1* gene.

Results

Case report

A 6-year-old boy with a high leukocyte count (64 700 μl^{-1}), containing 84% blasts in peripheral blood and with a mediastinal mass, was diagnosed as having T-ALL. A bone marrow smear was hypercellular with 69% blasts and negative for myeloperoxidase. The leukemic cells, after gating of CD45-positive cells, were positive for CD5 (90.7%), CD7 (90.7%), CD58 (69.9%) and cytoplasmic CD3 (92.8%), and negative for HLA-DR, IgG, IgM, Igκ, Igλ, CD8, CD13, CD14, CD19, CD20 and CD33. He was treated on the Tokyo Children's Cancer Study Group (TCCSG) L04-16 extremely high-risk (HEX) protocol, including stem cell transplantation, because the response to initial 7-day prednisolone (60 mg m^{-2}) monotherapy was poor. He achieved complete remission after the induction phase. After the early consolidation phase and two courses of the consolidation phase, he received allogeneic bone marrow transplantation from an unrelated HLA-matched donor 4 months after diagnosis. He has been in complete remission for 17 months.

The patient's leukemic cells at diagnosis were analysed after written informed consent was obtained from his parents, and the ethics committee of Kyoto Prefectural University of Medicine approved this study.

Identification of the AML1-LAF4 *fusion transcript*

Cytogenetic analysis of the leukemic cells of the patient using routine G-banding revealed 47, XY, add(1)(p36), +der(2)t(2;21)(q13;q22), t(2;21)(q13;q22), −9, −9, +mar1, +mar2, and spectral karyotyping (SKY) analysis revealed 47, XY, der(1)t(1;17)(p36.1;q23), der(2)t(2;21)(q11.2;q22), +der(2)t(2;21)(q11.2;q22), del(5)(p15.1), del(9)(q22), del(9)(p13), der(21)t(2;21)(q11.2;q22) (Supplementary Figure S1). Since *AML1* is located at 21q22, we inferred that *AML1* was rearranged in this case. Fluorescence *in situ* hybridization analysis using *AML1*-specific BAC (bacterial artificial chromosome) clones showed split signals of *AML1* on two der(2)t(2;21)(q11.2;q22) and der(21)t(2;21)(q11.2;q22) chromosomes (Figure 1a).

To isolate fusion transcripts of *AML1*, we performed the bubble PCR method for cDNA (Figure 2) and obtained various-sized products (Figure 3a). Four different-sized products were sequenced and two products contained *AML1* sequences fused to unknown sequences. Basic local alignment search tool (BLAST) search revealed that the unknown sequences were part of the *LAF4* gene and both products had the same in-frame junctions (Figure 3b). *LAF4* was located on chromosome 2q11.2–12, which was compatible with the result of spectral karyotyping analysis. We next performed reverse transcription-PCR to confirm *AML1-LAF4* fusion transcripts, and obtained three different-sized *AML1-LAF4* fusion products, including only one in-frame product (Figures 3c and d); however, reciprocal *LAF4-AML1* fusion transcripts were not generated (Figure 3c). Type 2 transcript is an out-of-frame fusion and generated premature termination in exon 9 of *LAF4* (Figure 3d). On the other hand, type 3 transcript is an in-frame fusion of exon 7 of *AML1* and exon 8 of *LAF4*, the same as the type 1 transcript; however, the type 3 transcript contained an 85-bp intronic sequence between exons 9 and 10 of *LAF4*, which might be due to splicing error, and appeared as a premature termination codon within the intronic sequences (Figure 3d). *AML1-LAF4* fusions were also confirmed by fluorescence *in situ* hybridization analysis (Figure 1b).

Detection of AML1-LAF4 *genomic junctions*

Southern blot analysis using a cDNA probe within exon 7 of *AML1* detected a rearranged band derived from an

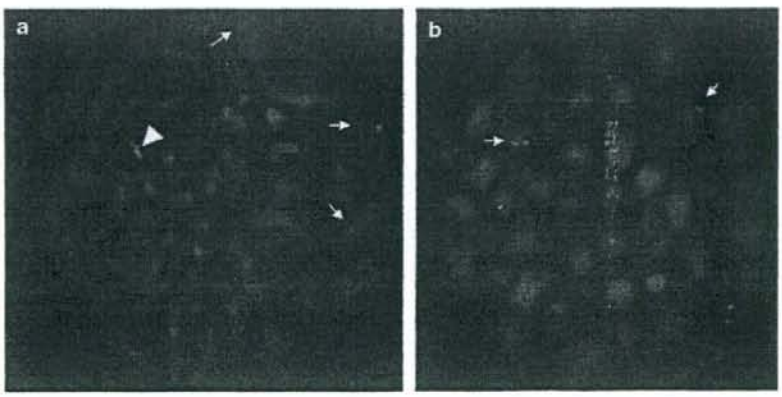

Figure 1 Fluorescence *in situ* hybridization analysis of the leukemic metaphase. (**a**) Both RP11-272A3 (green, 3′ side of *AML1*) and RP11-994N6 (red, 5′ side of *AML1*) were hybridized to normal chromosome 21 (arrowhead), RP11-272A3 to der(21)t(2;21)(q11.2;q22) (arrow, green signal) and RP11-994N6 to two der(2)t(2;21)(q11.2;q22) chromosomes (arrows, red signal). (**b**) Two fusion signals of RP11-994N6 (5′ of *AML1*, red signals) and RP11-527J8 (3′ of *LAF4*, green signals) were detected on two der(2)t(2;21)(q11.2;q22) chromosomes (arrows).

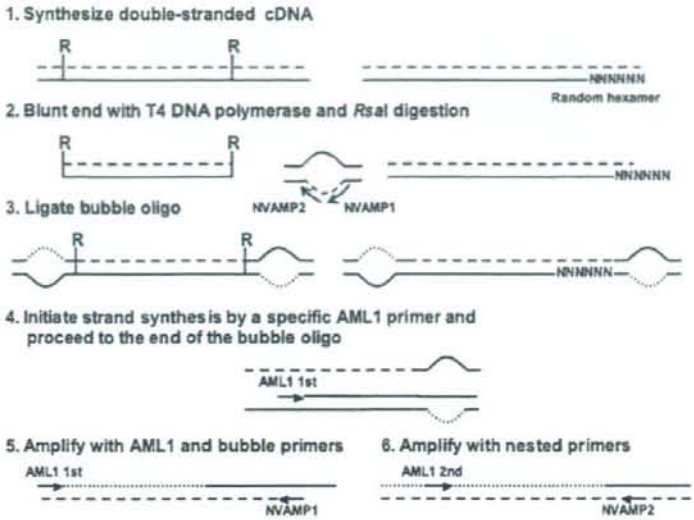

Figure 2 Outline of bubble PCR for cDNA. Bubble PCR primers (NVAMP-1 and NVAMP-2) can only anneal with one complementary sequence for bubble oligo synthesized with *AML1* primer, but not bubble oligo itself; therefore, this single-stranded bubble provides the specificity of the reaction.

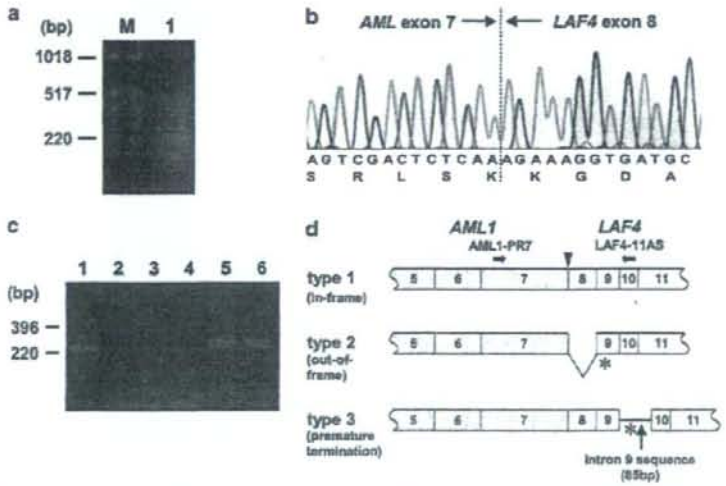

Figure 3 Identification of *AML1-LAF4* fusion transcript. (**a**) Bubble PCR products by nested PCR using AML1-5S and NVAMP1 for first PCR, and AML1-E6S and NVAMP2 for second PCR (lane 1). M, size marker. (**b**) Sequence analysis of *AML1-LAF4* fusion transcript. The single letter amino-acid sequences surrounding the fusion point are shown at the bottom of the figure. (**c**) Detection of *AML1-LAF4* fusion transcripts by reverse transcription-PCR. Primers were AML1-PR7 and LAF4-11AS (lanes 1 and 3), AML1-PR8 and LAF4-PR5 (lanes 2 and 4), and β-actin, respectively. Lanes 1, 3 and 5, patient's leukemic cells; lanes 2, 4 and 6, normal peripheral lymphocytes. (**d**) Three fusion transcripts of *AML1-LAF4* are schematically depicted. Gray/dotted boxes denote predicted *AML1* exons and white boxes represent predicted *LAF4* exons. Type 3 contains the *LAF4* intron 9 splicing donor site. AML1-PR7 and LAF4-11AS indicate the primers used for reverse transcription-PCR. Asterisk shows the termination codon.

approximately 11 kb *Bgl*II germline fragment on chromosome 21 (data not shown). To isolate the fusion point of chromosomes 2 and 21, we next performed bubble PCR on genomic DNA and detected nested PCR products using primers AML1-GNM8-2S and NVAMP2 (Figure 4a). Sequence analysis of the subcloned PCR product revealed the genomic junction of 5′-*AML1-LAF4*-3′ (Figures 4c and d), and the result

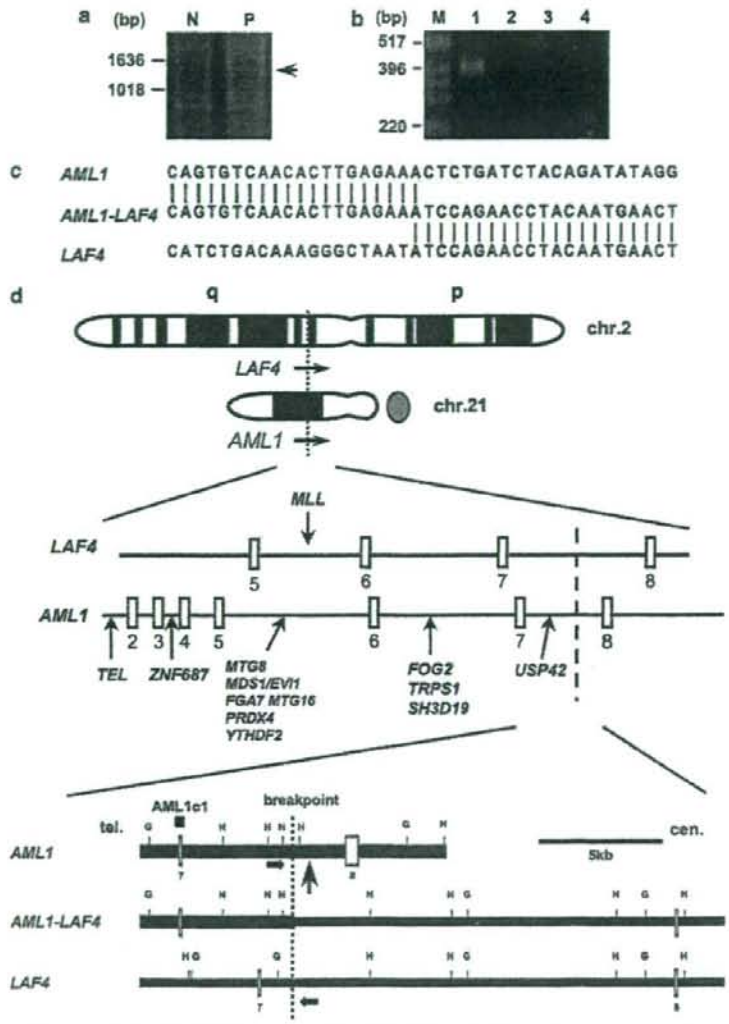

Figure 4 Cloning of the genomic junction of *AML1* and *LAF4*. (**a**) Bubble PCR for genomic DNA. N, normal human lymphocytes; P, patient's leukemic cells. (**b**) Detection of the genomic fusion point of *AML1-LAF4* by PCR. Primers were AML1-GNM8-4S and LAF4-GNM11-2AS (lanes 1 and 3), and LAF4-GNM11-2S and AML1-GNM8-2AS (lanes 2 and 4). Lanes 1 and 2, patient's leukemic cells; lanes 3 and 4, normal peripheral lymphocytes. M, size marker. (**c**) Sequences of breakpoints in the patient's leukemic cells. (**d**) Physical map of the breakpoint regions. Open vertical boxes represent defined exons in each gene. Horizontal arrows show the primers used. Restriction sites are indicated by capital letters: G, *Bgl*II; H, *Hind*III. AML1c1 indicates the position of the cDNA probes for Southern blot analysis. A vertical arrow shows *AML1-USP42* breakpoint.

was confirmed by PCR analysis using primers AML1-GNM8-4S and LAF4-GNM11-2AS (Figure 4b); however, no 5′-*LAF4-AML1*-3′ product was generated, suggesting interstitial deletion near genomic break points (Figure 4b). These sequences near the break points did not contain any lymphoid heptamer/nonamer sequences, *Alu* sequences or consensus topoisomerase II cleavage sites.

Discussion

In this study, we identified that *LAF4* was fused to *AML1* in pediatric T-ALL with t(2;21)(q11;q22). Other regions with chromosomal aberrations in this patient were not considered to be associated with recurrent cytogenetic changes involving T-ALL, except for the deletion of the short arm of chromosome 9. Spectral

karyotyping analysis detected del(9)(p13), and additional analysis of genome array (Human Mapping 50 K Hind Array, Affymetrix, Tokyo, Japan) revealed homozygous deletion of 4.5 Mb within the 9p21 region, including the *CDKN2A/p16/p14* locus (data not shown), which is frequently deleted in T-ALL (Ohnishi *et al.*, 1995).

Although the patient showed a complex chromosomal abnormality, t(2;21)(q11;q22) can form regular head-to-tail fusion transcripts of both *AML1* and *LAF4*, because the transcription direction of *AML1* and *LAF4* is telomere to centromere. Furthermore, fluorescence *in situ* hybridization analysis revealed two der(2)t(2;21)(q11.2;q22) creating 5′-*AML1-LAF4*-3′, suggesting that 5′-*AML1-LAF4*-3′ is critical for leukemogenesis.

LAF4 was previously reported to be a fusion partner of *MLL* in pediatric B-precursor ALL with t(2;21)(q11;q23) (von Bergh *et al.*, 2002; Bruch *et al.*, 2003; Hiwatari *et al.*, 2003). *LAF4* is the first gene fused to both *AML1* and *MLL*, and both *AML1-LAF4* and *MLL-LAF4* contained the same domains of *LAF4* (Figure 5). During the preparation of this manuscript, we found another pediatric T-ALL patient with *AML1-LAF4* reported in the Meeting Abstract (Abe *et al.*, *Blood* (ASH Annual Meeting Abstracts) 2006; **108**: 4276), suggesting that t(2;21)(q11;q23) is a recurrent cytogenetic abnormality and that the *AML1-LAF4* fusion gene is associated with the T-ALL phenotype. Both putative fusion proteins of AML1-LAF4 observed in two patients contained the Runt domain of AML1, and the transactivation domain, nuclear localization sequence and C-terminal homology domain of LAF4, although the fused exon of *LAF4* differed in the two cases. Several studies have reported that the fusion partners of *MLL* fused with different genes such as *MLL-AF10* and *CALM-AF10*, *MLL-CBP* and *MOZ-CBP* or *MLL-p300* and *MOZ-p300* (Ida *et al.*, 1997; Taki *et al.*, 1997; Chaffanet *et al.*, 2000). Comparison of the structure and function between *AML1-LAF4* and *MLL-LAF4* will facilitate our understanding of the molecular mechanisms underlying *AML1*- and *MLL*-related leukemia.

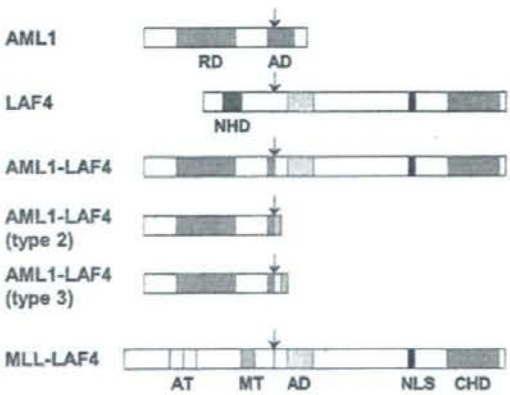

Figure 5 Schematic representation of putative AML1, LAF4 and AML1-LAF4 fusion proteins. Putative MLL-LAF4 fusion protein is also indicated for comparison. Arrows, break points or fusion points; AD, transactivation domain; AT, AT hooks; CHD, C-terminal homology domain; DNA, methyltransferase homology region; RD, RUNT domain; MT, DNA methyltransferase homology region; NLS, nuclear localization sequence.

The only *AML1* fusion partners in T-ALL are *LAF4* and *FGA7*. It is not known how *FGA7* is associated with T-ALL leukemogenesis, because *FGA7* does not show any significant sequence homology to any known protein motifs and/or domains (Mikhail *et al.*, 2004). Both patients with *AML1-LAF4* and *MLL-LAF4* fusions were diagnosed as having ALL, but they have different lymphoid lineages. *MLL-LAF4* is associated with B-lineage ALL; however, *AML1-LAF4* generates T-ALL. Our previous study showed that *LAF4* was expressed not only in B-lineage ALL but also in T-lineage ALL cell lines (Hiwatari *et al.*, 2003). *LAF4* showed strong sequence similarity to *AF4* (Ma and Staudt, 1996), which has a role in the differentiation of both B and T cells in mice (Isnard *et al.*, 2000). Furthermore, it was reported that *AML1* also plays an important role in T- and B-cell differentiation, because *AML1*-deficient bone marrow increased defective T- and B-lymphocyte development (Ichikawa *et al.*, 2004). These findings support that both *AML1* and *LAF4* are associated with T-ALL, respectively. Further functional analysis of the *AML1-LAF4* fusion gene will provide new insights into the leukemogenesis of *AML1*-related T-ALL. Recently, it has been reported that C-terminal truncated AML1-related fusion proteins play critical roles in leukemogenesis (Yan *et al.*, 2004, Agerstam *et al.*, 2007), suggesting that the two additional types of fusion transcripts observed in our patient (types 2 and 3 in Figures 3d and 5) have an additional function in leukemogenesis other than that of the entire AML1-LAF4 fusion protein.

In this study, we first applied the panhandle PCR method, which is usually used for cloning the fusion partners of *MLL* or *NUP98* (Megonigal *et al.*, 2000; Taketani *et al.*, 2002); however, no fusion transcripts could be obtained. Therefore, we searched for another method to clone the fusion transcripts and adapted the bubble PCR method for cDNA cloning. To date, bubble PCR has been performed for cloning unknown genomic fusion points but not fusion cDNAs (Zhang *et al.*, 1995). Using double-stranded cDNA, we could apply the bubble PCR method for cloning fusion cDNA with fewer nonspecific products. The bubble PCR primer can only prime DNA synthesis after a first-strand cDNA has been generated by an *AML1*-specific primer because of the bubble-tag with an internal non-complementary region (Zhang *et al.*, 1995). Although bubble PCR for genomic DNA generated one or two amplification products (Smith, 1992), bubble PCR for cDNA generated a complex set of amplification products that appeared as a smear by SYBR green staining, suggesting that a random hexamer generated various double-stranded cDNA containing the *AML1* sequence. This means that various fusion points can be estimated, even if after bubble oligo ligation was generated. Furthermore, bubble PCR for cDNA could amplify in both 5′–3′ and 3′–5′ directions of the gene or transcript, and easily

Table 1 Comparison between bubble PCR and panhandle PCR

Characteristics	*Bubble PCR*	*Panhandle PCR*
Available orientation of fusion transcript	5′–3′, 3′–5′	Only 5′–3′
AML1-specific random hexamer[a]	Not necessary	Necessary
Self-annealing	Not necessary	Necessary
Number of required polymerase reaction	2	4
Number of final products	Many (smear)	A few
Nonspecific product	Few	Few
Number of extra sequences other than targeted sequences in cloned product	50–60 bp	> 100 bp
Search for other targeted exons	Easy	Hard[b]

[a]30-mers *AML1*-specific oligonucleotide with random hexamer (AML1-N). [b]Necessary to use another *AML1*-specific random hexamer if the target exons are 5′ region of the initial target.

handle any exons fused to unknown partners for amplification. Once-ligated cDNAs are also available for cloning any genes, other than *AML1*, as the target. We demonstrated the efficiency and specificity of bubble PCR for cDNA (Table 1 and Supplementary Figure S2).

To date, a great number of fusion genes associated with chromosomal translocations have been cloned, although these fusion genes are found as a minor part of various malignancies. Recently, high frequencies of mutations in *NOTCH1* in T-ALL (James *et al.*, 2005), *NPM* in AML with normal karyotype (Weng *et al.*, 2004) and *JAK2* in myeloproliferative disorders (polycythemia vera, essential thrombocythemia and idiopathic myelofibrosis) (James *et al.*, 2005) have been reported, and these mutations are considered to be a good target for therapy. These genes were first identified as associated with chromosomal translocations in a small subset of specific phenotypes of hematologic malignancies (Ellisen *et al.*, 1991; Morris *et al.*, 1994; Lacronique *et al.*, 1997). These findings suggest that continuing attempts to identify genes associated with chromosomal translocations can be expected to provide further insights into the significance of various gene alterations in cancer and the development of novel-targeted therapies (Taki and Taniwaki, 2006). The bubble PCR method for cDNA will contribute to identifying numerous novel translocation partners more easily and further functional analysis of chimeric transcripts.

Materials and methods

Spectral karyotyping analysis
Spectral karyotyping analysis was performed with a Sky-Painting kit (Applied Spectral Imaging, Migdal Ha'Emek, Israel). Signal detection was performed according to the manufacturer's instructions.

Fluorescence in situ *hybridization analysis*
Fluorescence *in situ* hybridization analysis of the patient's leukemic cells using *AML1*-specific BAC clones (RP11-272A3, 3′ of *AML1* and RP11-994N6, 5′ of *AML1*) was carried out as described previously (Taniwaki *et al.*, 1994). Fusion of *AML1* and *LAF4* was analysed with the patient's leukemic cells using RP11-994N6 (5′ of *AML1*) and RP11-527J8 (3′ of *LAF4*).

Bubble PCR for cDNA
We modified the original bubble PCR method to apply for cDNA cloning (Figure 2; Supplementary Figure S2) (Smith, 1992; Zhang *et al.*, 1995).

Poly(A)$^+$ RNA was extracted from the patient's leukemic cells using a QuickPrep Micro mRNA Purification Kit (GE Healthcare, Buckinghamshire, UK). Two hundred nanograms of poly(A)$^+$ RNA was reverse transcribed to cDNA in a total volume of 33 µl with random hexanucleotide using the Ready-To-Go You-Prime First-Strand Beads (GE Healthcare). Double-stranded cDNAs were synthesized from 10 µl of single-stranded cDNA with a phosphorylated random hexanucleotide, blunt ended with T4 DNA polymerase, digested with *Rsa*I endonuclease and ligated with bubble oligo. *Rsa*I, a 4-bp blunt-ended cutter, was chosen to shorten the bubble oligo-ligated fragments, so that almost all bubble oligo-ligated fragments would be easy to clone by standard PCR reaction. This suggests that poor-quality samples are also suited to this method, although it is unsuitable for cloning long products.

The sequences of the primers used are listed in Supplementary Table S1 and their positions in the *AML1* gene are shown in Supplementary Figure S2. Nested PCR was performed using primers NVAMP-1 (bubble oligo) and AML1-5S (exon 5) for first round PCR, and NVAMP-2 (bubble oligo) and AML1-E6S (exon 6) for nested PCR. NVAMP1 and NVAMP2 can only anneal to the newly synthesized unique sequence of the bubble oligo by AML1-5S.

We used poly(A)$^+$ RNA in bubble PCR for cDNA with the expectation that this approach could amplify fewer transcripts; however, total RNA is also suitable for this method.

Bubble PCR for genomic DNA
Bubble PCR for genomic DNA was performed as described previously (Smith, 1992; Zhang *et al.*, 1995). Primers were as follows: NVAMP-1 and AML1-GNM8S for first round PCR, and NVAMP-2 and AML1-GNM8-2S for second round PCR (Supplementary Table S1).

Reverse transcription–PCR and genomic PCR analyses
Reverse transcription–PCR and genomic PCR analyses were performed as described previously. After 35 rounds of PCR (30 s at 94 °C, 30 s at 55 °C, 1 min at 72 °C), 5µl of PCR product were electrophoresed in a 3% agarose gel. Primers were as follows: AML1-PR7 and LAF4-11AS, and AML1-PR8 and LAF4-PR5 for reverse transcription-PCR; and AML1-GNM8-4S and LAF4-GNM11-2AS, and LAF4-GNM11-2S and AML1-GNM8-2AS for genomic PCR (Supplementary Table S1).

Nucleotide sequencing
Nucleotide sequences of PCR products and, if necessary, subcloned PCR products were analysed as described previously (Hiwatari *et al.*, 2003).

Southern blot analysis
High-molecular-weight DNA was extracted from the patient's leukemic cells by proteinase K digestion and phenol/chloroform extraction. DNA (10 µg) was digested with *Bgl*II, subjected to electrophoresis on 0.7% agarose gel and transferred to a nylon membrane. Blots were hybridized to probes that were labeled by the Dig-labeled PCR method according to the manufacturer's instructions (Roche Applied Science, Tokyo, Japan). Probes

were 112 bp *AML1* cDNA fragments (AML1c1, nucleotides 1233–1344; GenBank accession no. NM_001754).

Abbreviations

AML, acute myeloid leukemia; ALL, acute lymphoblastic leukemia.

Acknowledgements

We express our appreciation for the outstanding technical assistance of Kozue Sugimoto, Minako Goto and Kayoko Kurita. This work was supported by a grant-in-aid for Scientific Research (B) from the Ministry of Education, Culture, Sports, Science and Technology of Japan, and the Takeda Science Foundation.

References

Agerstam H, Lilljebjorn H, Lassen C, Swedin A, Richter J, Vandenberghe P *et al.* (2007). Fusion gene-mediated truncation of *RUNX1* as a potential mechanism underlying disease progression in the 8p11 myeloproliferative syndrome. *Genes Chromosomes Cancer* **46**: 635–643.

Asou N, Yanagida M, Huang L, Yamamoto M, Shigesada K, Mitsuya H *et al.* (2007). Concurrent transcriptional deregulation of AML1/RUNX1 and GATA factors by the *AML1-TRPS1* chimeric gene in t(8;21)(q24;q22) acute myeloid leukemia. *Blood* **109**: 4023–4027.

Bruch J, Wilda M, Teigler-Schlegel A, Harbott J, Borkhardt A, Metzler M. (2003). Occurrence of an *MLL/LAF4* fusion gene caused by the insertion ins(11;2)(q23;q11.2q11.2) in an infant with acute lymphoblastic leukemia. *Genes Chromosomes Cancer* **37**: 106–109.

Chaffanet M, Gressin L, Preudhomme C, Soenen-Cornu V, Birnbaum D, Pebusque MJ. (2000). *MOZ* is fused to *p300* in an acute monocytic leukemia with t(8;22). *Genes Chromosomes Cancer* **28**: 138–144.

Chan EM, Comer EM, Brown FC, Richkind KE, Holmes ML, Chong BH *et al.* (2005). *AML1-FOG2* fusion protein in myelodysplasia. *Blood* **105**: 4523–4526.

Ellisen LW, Bird J, West DC, Soreng AL, Reynolds TC, Smith SD *et al.* (1991). *TAN-1*, the human homolog of the Drosophila *Notch* gene, is broken by chromosomal translocations in T lymphoblastic neoplasms. *Cell* **66**: 649–661.

Erickson P, Gao J, Chang KS, Look T, Whisenant E, Raimondi S *et al.* (1992). Identification of breakpoints in t(8;21) acute myelogenous leukemia and isolation of a fusion transcript, AML1/ETO, with similarity to *Drosophila* segmentation gene, runt. *Blood* **80**: 1825–1831.

Gamou T, Kitamura E, Hosoda F, Shimizu K, Shinohara K, Hayashi Y *et al.* (1998). The partner gene of *AML1* in t(16;21) myeloid malignancies is a novel member of the *MTG8* (*ETO*) family. *Blood* **91**: 4028–4037.

Golub TR, Barker GF, Bohlander SK, Hiebert SW, Ward DC, Bray-Ward P *et al.* (1995). Fusion of the *TEL* gene on 12p13 to the *AML1* gene on 21q22 in acute lymphoblastic leukemia. *Proc Natl Acad Sci USA* **92**: 4917–4921.

Grimwade D, Walker H, Oliver F, Wheatley K, Harrison C, Harrison G *et al.* (1998). The importance of diagnostic cytogenetics on outcome in AML: analysis of 1,612 patients entered into the MRC AML 10 trial. The Medical Research Council Adult and Children's Leukaemia Working Parties. *Blood* **92**: 2322–2333.

Hayashi Y. (2000). The molecular genetics of recurring chromosome abnormalities in acute myeloid leukemia. *Semin Hematol* **37**: 368–380.

Hiwatari M, Taki T, Taketani T, Taniwaki M, Sugita K, Okuya M *et al.* (2003). Fusion of an *AF4*-related gene, *LAF4*, to *MLL* in childhood acute lymphoblastic leukemia with t(2;11)(q11;q23). *Oncogene* **22**: 2851–2855.

Ichikawa M, Asai T, Saito T, Seo S, Yamazaki I, Yamagata T *et al.* (2004). *AML-1* is required for megakaryocytic maturation and lymphocytic differentiation, but not for maintenance of hematopoietic stem cells in adult hematopoiesis. *Nat Med* **10**: 299–304.

Ida K, Kitabayashi I, Taki T, Taniwaki M, Noro K, Yamamoto M *et al.* (1997). Adenoviral E1A-associated protein p300 is involved in acute myeloid leukemia with t(11;22)(q23;q13). *Blood* **90**: 4699–4704.

Isnard P, Core N, Naquet P, Djabali M. (2000). Altered lymphoid development in mice deficient for the m*AF4* proto-oncogene. *Blood* **96**: 705–710.

James C, Ugo V, Le Couedic JP, Staerk J, Delhommeau F, Lacout C *et al.* (2005). A unique clonal *JAK2* mutation leading to constitutive signalling causes polycythaemia vera. *Nature* **434**: 1144–1148.

Kurokawa M, Hirai H. (2003). Role of AML1/Runx1 in the pathogenesis of hematological malignancies. *Cancer Sci* **94**: 841–846.

Lacronique V, Boureux A, Valle VD, Poirel H, Quang CT, Mauchauffe M *et al.* (1997). A TEL-JAK2 fusion protein with constitutive kinase activity in human leukemia. *Science* **278**: 1309–1312.

Ma C, Staudt LM. (1996). *LAF-4* encodes a lymphoid nuclear protein with transactivation potential that is homologous to *AF-4*, the gene fused to *MLL* in t(4;11) leukemias. *Blood* **87**: 734–745.

Megonigal MD, Rappaport EF, Wilson RB, Jones DH, Whitlock JA, Ortega JA *et al.* (2000). Panhandle PCR for cDNA: a rapid method for isolation of *MLL* fusion transcripts involving unknown partner genes. *Proc Natl Acad Sci USA* **97**: 9597–9602.

Mikhail FM, Coignet L, Hatem N, Mourad ZI, Farawela HM, El Kaffash DM *et al.* (2004). *FGA7*, is fused to *RUNX1/AML1* in a t(4;21)(q28;q22) in a patient with T-cell acute lymphoblastic leukemia. *Genes Chromosomes Cancer* **39**: 110–118.

Mitani K, Ogawa S, Tanaka T, Miyoshi H, Kurokawa M, Mano H *et al.* (1994). Generation of the *AML1-EVI-1* fusion gene in the t(3;21)(q26;q22) causes blastic crisis in chronic myelocytic leukemia. *EMBO J* **13**: 504–510.

Miyoshi H, Kozu T, Shimizu K, Enomoto K, Maseki N, Kaneko Y *et al.* (1993). The t(8;21) translocation in acute myeloid leukemia results in production of an *AML1-MTG8* fusion transcript. *EMBO J* **12**: 2715–2721.

Miyoshi H, Shimizu K, Kozu T, Maseki N, Kaneko Y, Ohki M. (1991). t(8;21) breakpoints on chromosome 21 in acute myeloid leukemia are clustered within a limited region of a single gene, *AML1*. *Proc Natl Acad Sci USA* **88**: 10431–10434.

Morris SW, Kirstein MN, Valentine MB, Dittmer KG, Shapiro DN, Saltman DL *et al.* (1994). Fusion of a kinase gene, *ALK*, to a nucleolar protein gene, *NPM*, in non-Hodgkin's lymphoma. *Science* **263**: 1281–1284.

Nguyen TT, Ma LN, Slovak ML, Bangs CD, Cherry AM, Arber DA. (2006). Identification of novel *Runx1* (*AML1*) translocation partner genes *SH3D19*, *YTHDf2*, and *ZNF687* in acute myeloid leukemia. *Genes Chromosomes Cancer* **45**: 918–932.

Ohnishi H, Kawamura M, Ida K, Sheng XM, Hanada R, Nobori T *et al.* (1995). Homozygous deletions of *p16/MTS1* gene are frequent but mutations are infrequent in childhood T-cell acute lymphoblastic leukemia. *Blood* **86**: 1269–1275.

Okuda T, Cai Z, Yang S, Lenny N, Lyu CJ, van Deursen JM *et al.* (1998). Expression of a knocked-in *AML1-ETO* leukemia gene inhibits the establishment of normal definitive hematopoiesis and directly generates dysplastic hematopoietic progenitors. *Blood* **91**: 3134–3143.

Paulsson K, Bekassy AN, Olofsson T, Mitelman F, Johansson B, Panagopoulos I. (2006). A novel and cytogenetically cryptic t(7;21)(p22;q22) in acute myeloid leukemia results in fusion of *RUNX1* with the ubiquitin-specific protease gene *USP42*. *Leukemia* **20**: 224–229.

Rowley JD. (1999). The role of chromosome translocations in leukemogenesis. *Semin Hematol* **36**: 59–72.

Smith DR. (1992). Ligation-mediated PCR of restriction fragments from large DNA molecules. *PCR Methods Appl* **2**: 21–27.

Taketani T, Taki T, Shibuya N, Ito E, Kitazawa J, Terui K *et al.* (2002). The *HOXD11* gene is fused to the *NUP98* gene in acute myeloid leukemia with t(2;11)(q31;p15). *Cancer Res* **62**: 33–37.

Taki T, Sako M, Tsuchida M, Hayashi Y. (1997). The t(11;16)(q23;p13) translocation in myelodysplastic syndrome fuses the *MLL* gene to the *CBP* gene. *Blood* **89**: 3945–3950.

Taki T, Taniwaki M. (2006). Chromosomal translocations in cancer and their relevance for therapy. *Curr Opin Oncol* **18**: 62–68.

Taniwaki M, Matsuda F, Jauch A, Nishida K, Takashima T, Tagawa S *et al.* (1994). Detection of 14q32 translocations in B-cell malignancies by *in situ* hybridization with yeast artificial chromosome clones containing the human IgH gene locus. *Blood* **83**: 2962–2969.

Von Bergh AR, Beverloo HB, Rombout P, van Wering ER, van Weel MH, Beverstock GC *et al.* (2002). *LAF4*, an *AF4*-related gene, is fused to *MLL* in infant acute lymphoblastic leukemia. *Genes Chromosomes Cancer* **37**: 106–109.

Wang J, Hoshino T, Redner RL, Kajigaya S, Liu JM. (1998). *ETO*, fusion partner in t(8;21) acute myeloid leukemia, represses transcription by interaction with the human N-CoR/mSin3/HDAC1 complex. *Proc Natl Acad Sci USA* **95**: 10860–10865.

Weng AP, Ferrando AA, Lee W, Lee W, Morris IV JP, Silverman LB *et al.* (2004). Activating mutations of *NOTCH1* in human T cell acute lymphoblastic leukemia. *Science* **306**: 269–271.

Yan M, Burel SA, Peterson LF, Kanbe E, Iwasaki H, Boyapati A *et al.* (2004). Deletion of an AML1-ETO C-terminal NcoR/SMRT-interacting region strongly induces leukemia development. *Proc Natl Acad Sci USA* **101**: 17186–17191.

Zhang JG, Goldman JM, Cross NC. (1995). Characterization of genomic *BCR-ABL* breakpoints in chronic myeloid leukemia by PCR. *Br J Haematol* **90**: 138–146.

Zhang Y, Emmanuel N, Kamboj G, Chen J, Shurafa M, Van Dyke DL *et al.* (2004). *PRDX4*, a member of the peroxiredoxin family, is fused to *AML1* (*RUNX1*) in an acute myeloid leukemia patient with a t(X;21)(p22;q22). *Genes Chromosomes Cancer* **40**: 365–370.

Supplementary Information accompanies the paper on the Oncogene website (http://www.nature.com/onc).

Down-regulation of TCF8 is involved in the leukemogenesis of adult T-cell leukemia/lymphoma

*Tomonori Hidaka,[1,2] *Shingo Nakahata,[1] *Kinta Hatakeyama,[3] Makoto Hamasaki,[1,4] Kiyoshi Yamashita,[2] Takashi Kohno,[5] Yasuhito Arai,[6] Tomohiko Taki,[7] Kazuhiro Nishida,[7] Akihiko Okayama,[8] Yujiro Asada,[3] Ryoji Yamaguchi,[9] Hirohito Tsubouchi,[2,10] Jun Yokota,[5] Masafumi Taniwaki,[7] Yujiro Higashi,[11] and Kazuhiro Morishita[1]

[1]Division of Tumor and Cellular Biochemistry, Department of Medical Sciences, [2]Department of Internal Medicine II, University of Miyazaki, Miyazaki, [3]First Department of Pathology, Faculty of Medicine, University of Miyazaki, Miyazaki; [4]Miyazaki Prefectural Industrial Foundation, Miyazaki; [5]Biology Division, National Cancer Center Research Institute, Tokyo; [6]Cancer Genome Project, National Cancer Center Research Institute, Tokyo; [7]Department of Hematology and Oncology, Kyoto Prefectural University of Medicine, Kyoto; [8]Department of Rheumatology, Infectious Diseases and Laboratory Medicine, University of Miyazaki, Miyazaki; [9]Department of Veterinary Pathology, University of Miyazaki, Miyazaki; [10]Department of Digestive and Life-style related Disease, Kagoshima University Graduate School of Medicine and Dental Sciences, Kagoshima; and [11]Graduate School of Frontier Biosciences, Osaka University, Osaka, Japan

Adult T-cell leukemia/lymphoma (ATLL) is caused by latent human T-lymphotropic virus-1 (HTLV-1) infection. To clarify the molecular mechanism underlying leukemogenesis after viral infection, we precisely mapped 605 chromosomal breakpoints in 61 ATLL cases by spectral karyotyping and identified frequent chromosomal breakpoints in 10p11, 14q11, and 14q32. Single nucleotide polymorphism (SNP) array–comparative genomic hybridization (CGH), genetic, and expression analyses of the genes mapped within a common breakpoint cluster region in 10p11.2 revealed that in ATLL cells, transcription factor 8 *(TCF8)* was frequently disrupted by several mechanisms, including mainly epigenetic dysregulation. *TCF8* mutant mice frequently developed invasive CD4+ T-cell lymphomas in the thymus or in ascitic fluid in vivo. Down-regulation of TCF8 expression in ATLL cells in vitro was associated with resistance to transforming growth factor β1 (TGF-β1), a well-known characteristic of ATLL cells, suggesting that escape from TGF-β1–mediated growth inhibition is important in the pathogenesis of ATLL. These findings indicate that *TCF8* has a tumor suppressor role in ATLL. (Blood. 2008;112:383-393)

Introduction

Adult T-cell leukemia/lymphoma (ATLL) is a peripheral CD4+ T-cell malignancy caused by infection with human T-lymphotropic virus-1 (HTLV-1).[1] HTLV-1 infection is endemic in a number of well-defined geographic regions within Japan, and as many as 20 million individuals worldwide are estimated to harbor it.[2] ATLL occurs after a prolonged latency period of up to 50 years in approximately 5% of individuals who have been infected with HTLV-1 around the time of birth. HTLV-1 encodes a transactivator, *Tax*, which plays a key role in the polyclonal growth of infected T cells through the activation of various genes.[3] However, recent studies have shown that Tax expression is undetectable in circulating ATLL cells, while a genetically and epigenetically defective provirus was observed in more than half of the ATLL patients examined.[4,5] Considering the long latency period of ATLL, it has been proposed that at least 5 additional genetic or epigenetic events are required for the development of overt disease.[1,6]

Nonrandom chromosomal translocations are considered to cause leukemic transformation, including structural and/or quantitative abnormalities of transcription factors such as *AML1*, *EVI1*, and *MLL*.[7] To identify disease-specific chromosomal translocations in ATLL, karyotypes of 107 ATLL cases determined by the G-banding method were reviewed in Japan.[8] There was a high degree of diversity and complexity, and disease-specific translocations were not found; however, translocations involving 14q32 (28%) or 14q11 (14%) and the deletion of 6q (23%) were the most frequent chromosomal abnormalities.[8] Recently, chromosome-based comparative genomic hybridization (CGH)[9] and BAC array-based CGH showed complex chromosomal abnormalities with gains in 1q, 2p, 4q, 7p, and 7q, and losses in 10p, 13q, 16q, and 18p.[10] To date, however, no gene involved in the development of ATLL has been isolated. Array CGH is useful for detecting genomic deletions or amplifications, but it cannot detect chromosomal translocations or inversions.

In this study, we searched for the existence of recurrent chromosomal rearrangements by multicolor spectral karyotyping (SKY) and high-resolution single nucleotide polymorphism (SNP) array-CGH (SNP array-CGH). We precisely mapped 605 chromosomal breakpoints in 61 ATLL cases. Breakpoints occurred most frequently in 10p11 and were mapped within a 1-Mb region in 10p11.2 with heterozygous deletions in all cases. A minimal common region of chromosome deletions, including a region of homozygous deletion, was mapped to a 2-Mb region. Genetic and expression analyses of the genes mapped within the deleted region revealed transcription factor 8 *(TCF8)* to be frequently altered in ATLL cells by several mechanisms, including mainly epigenetic dysregulation, suggesting that *TCF8* may be a candidate tumor suppressor gene. *TCF8* (GenBank accession number, NM 030751[11]), *AREB6*, *ZFHEP*, *NIL-2A*, *ZFHX1A*, *NIL-2-A*, *MGC133261*, or

Submitted January 5, 2008; accepted April 4, 2008. Prepublished online as *Blood* First Edition paper, May 8, 2008; DOI 10.1182/blood-2008-01-131185.

*T.H., S.N., and K.H. contributed equally to this paper.

The online version of this article contains a data supplement.

The publication costs of this article were defrayed in part by page charge payment. Therefore, and solely to indicate this fact, this article is hereby marked "advertisement" in accordance with 18 USC section 1734.

ZEB1 encodes a 2-handed zinc finger homeodomain protein,[12] which represents a key player in pathogenesis associated with tumor progression in solid cancers.[13,14] In this study, we found that *TCF8* mutant mice frequently developed CD4+ T-cell lymphoma/leukemia half a year after birth. Furthermore, we showed that down-regulation of TCF8 expression in ATLL cells in vitro was associated with TGF-β1 resistance, a well-known characteristic of ATLL cells, suggesting that escape from TGF-β1–mediated growth inhibition is one of the primary mechanisms in the pathogenesis of ATLL. These findings suggest that *TCF8* has an important tumor suppressor role in ATLL.

Methods

Patient samples

ATLL cells were collected from patients at the time of admission to hospital and before chemotherapy.[15] Diagnosis of ATLL was made on the basis of clinical features, hematologic characteristics, serum antibodies against HTLV-1 antigens, and insertion of the HTLV-1 viral genome into leukemia cells by Southern blot hybridization. Using Shimoyama's criteria,[16] all patients were diagnosed as acute-type ATLL. Mononuclear cells were obtained from heparinized blood or ascites by Histopaque density gradient centrifugation (Sigma-Aldrich, St Louis, MO). After separation, ATLL cell enrichment of more than 90% was confirmed by 2-color flow cytometric analysis. All samples were separated by Histopaque density gradient centrifugation, quickly frozen within 3 hours, and cryopreserved at −80°C. This study was approved by the Institutional Review Board of the Faculty of Medicine, University of Miyazaki. Informed consent was obtained from all blood and tissue donors in accordance with the Declaration of Helsinki.

Cell lines

Acute lymphoblastic leukemia (ALL) cell lines used in this study were described previously.[15] Briefly, 4 of the cell lines, Jurkat, MOLT4, MKB1, and KAWAI, are HTLV-1–negative human T-cell acute lymphoblastic leukemia (T-ALL) cell lines.[17,18] Three cell lines, KOB, SO4, and KK1, are interleukin 2 (IL2)–dependent ATLL cell lines.[19] ED, Su9T, and S1T are IL2-independent ATLL cell lines.[20] MT2 and HUT102 are human T-cell lines transformed by HTLV-1 infection.[21] CTLL2 is a murine IL2–dependent T-lymphoma cell line.[22] All the cell lines were maintained in RPMI1640 medium supplemented with 10% fetal calf serum (FCS) and with or without IL2.

Cell culture and karyotype analysis

G-banding studies were performed as described previously.[8] Briefly, leukemia cells were diluted in 10 mL RPMI1640 medium supplemented with 10% FCS at a final concentration of 10^6 cells/mL. The cells were cultured at 37°C for 24 to 48 hours in humidified air with 5% CO_2, exposed to colcemid (0.05 mg/mL) for 60 minutes, processed in 0.075 M potassium chloride for 20 minutes, and fixed with methanol/glacial acetate (3:1). The chromosomes were treated with trypsin, stained with a Giemsa solution, and karyotyped according to the International System for Human Cytogenetic Nomenclature (ISCN 2005).[23] The remaining chromosome pellets were stored at −20°C for SKY and fluorescence in situ hybridization (FISH) analyses.

SKY and DAPI banding analysis

The strategy of combined spectral karyotyping (SKY) and 4,6-diaminido-2-phenylindole dihydrochloride (DAPI) banding analysis of chromosome abnormalities was published[24] and is briefly described as follows: The chromosomes prepared on a slide glass were denatured and hybridized with a cocktail probe mixture for 2 days at 37°C. The SKY probe mixture and hybridization reagents were purchased from Applied Spectral Imaging (Vista, CA), and signal detection was performed according to the manufacturer's protocol. The chromosomes were counterstained with DAPI combined with an antifade solution (Vectashield; Vector Laboratories, Burlingame, CA). Images were acquired by an SD200 Spectracube (Applied Spectral Imaging) mounted on an Olympus BX50-RF (Olympus, Tokyo, Japan) using a custom-designed optical filter (SKY-1; Chroma Technology, San Diego, CA). With another special optical filter, the inverted DAPI images were captured in conjunction with spectral classifications as QFH band patterns for the identification of chromosomal breakpoints. For each case, 10 to 20 metaphase spreads were analyzed, and karyotypes were described according to the ISCN 2005.[23]

FISH analysis

The plasmid library from sorted human chromosomes 10 (pBS10) was used as a whole chromosome painting (WCP) probe, labeled with digoxigenin-16-dUTP (Boehringer-Ingelheim, Ingelheim, Germany) by standard nick translation. BAC clones were labeled with biotin-16-dUTP (Sigma-Aldrich). Hybridization and signal detection were performed as described previously.[25] A minimum of 50 nuclei was examined for each FISH. FISH analysis was performed on metaphase and interphase chromosomes by 53 BAC clones mapped to the chromosome bands 10p11-12 in the human genome mapping of NCBI (build 36 version 1)[26] as probes.

High-density SNP array comparative genomic hybridization (array-CGH) analysis

Total genomic DNA was digested with *XbaI*, ligated to an adaptor, and subjected to polymerase chain reaction (PCR) amplification using a single primer. After treatment with DNase I, 40 μg of the PCR products was labeled with a biotinylated nucleotide analog and hybridized the microarray. SNP genotypes were scored with the GTYPE 4.1 software (Affymetrix, Santa Clara, CA). Chromosome copy number and LOH were calculated with 2 programs, ACUE 2.1 (Mitsui Knowledge Industry, Tokyo, Japan, http://bio.mki.co.jp/en/product/acue2/index.html) and CNAG 2.0 (Affymetrix).[27] For data normalization, we used 6 normal reference samples. Genomic location of probes on the array was determined with the information in NCBI genome map build 35.1.[26]

Mice

C57BL/6 and ICR mice were purchased from CLEA Japan (Tokyo, Japan) and maintained under specific pathogen-free conditions. The targeted allele of the δ*EF1* gene, the murine orthologue of *TCF8*, lacks only the COOH-proximal zinc finger cluster domain.[28] Approximately 20% of the homozygous *TCF8* mutant mice were born alive and grew up to adulthood, although it was reported to cause a defect in the thymic T-cell development.[28,29] To produce viable homozygous *TCF8* mutant mice, we made their genetic backgrounds more heterogeneous by crossing the C57BL/6 background *TCF8* mutant mice with the ICR outbred strain or F1 (C57BL/6 × C3H) mice.

Assay for cell proliferation

Control siRNA was purchased from Qiagen (Valencia, CA; AllStars Negative Control [ANC] siRNA) and the *TCF8* siRNA was from Ambion (Austin, TX; murine *TCF8*: 5′-CCUGUGGAUUAUGAGUUCA-3′, human *TCF8* 5′-GGGUUACUUGUACACAGCU-3′). For the construction of vectors expressing TCF8, human *TCF8* cDNA was subcloned into pCMV26 (Sigma-Aldrich). The cells were transiently transfected using the Nucleofector Kit (Amaxa, Gaithersburg, MD) according to the manufacturer's recommendations. The transfection efficiency, evaluated by fluorescence microscopy of green fluorescent protein, was more than 80%. Twenty-four hours after transfection, the expression of TCF8 protein in the cells was investigated by Western blotting, while for the cell proliferation studies, each transfectant was plated at a density of 4×10^3 cells per well in 96-well microtiter plates. The cells were treated with various concentrations of transforming growth factor (TGF-β1; R&D Systems, Minneapolis, MN) for 72 hours and counted by the methyl thiazolyl tetrazolium (MTT) assay

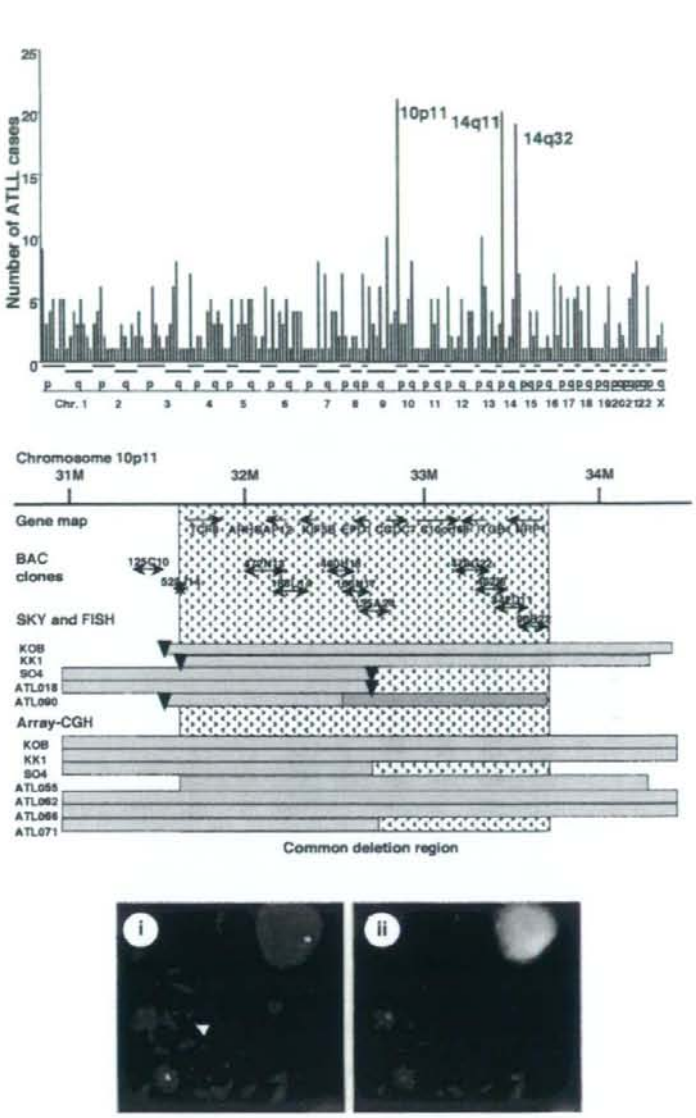

Figure 1. Mapping of the deletions at 10p11.2. (A) Mapping of the chromosomal breakpoints in whole chromosomes in acute-type ATLLs. An analysis of the chromosomal breakpoints was performed by spectral karyotyping (SKY), and all chromosomal breakpoints were mapped in each region of the chromosomes (x-axis), as indicated at the bottom. The y-axis shows the numbers of ATLL cases with the chromosomal breakpoints in each chromosomal region. Three regions, 10p11, 14q11, and 14q32, were frequently identified with chromosomal breakpoints. (B) Physical and transcriptional maps of the region containing the chromosomal deletion at 10p11. A FISH analysis was performed on metaphase and interphase chromosomes using 53 BAC clones mapped to the chromosome bands at 10p11-12 in the human genome map of NCBI (build 36 version 1[28]) as probes. The bars indicate the region covering each BAC clone. Horizontal bars indicate the region with hemizygous deletions in each DNA sample from the ATLL cell lines or ATLL cells from patients, which were detected by SKY and FISH or array-CGH analyses. The inverted triangles indicate the regions of chromosomal breakpoints. Closed bars indicate the region of a homozygous deletion in a DNA sample from ATLL cells (ATL090). The hatch pattern represents the minimal heterozygous deletion at 10p11.2. *TCF8* through *NRP1* represent the names of the genes within the region in the human genome map of NCBI (build 36 version 1[28]). (C) FISH validation of the RP11-188L14 probe to detect the hemizygous deletion of the chromosome10p11.2 in SO4 cell line. The RP11-188L14 probe was green (FITC) and the whole chromosome painting probe was red (TRITC). FISH with RP11-188L14 shows no signal on the abnormal chromosome 10 as indicated by the arrow (i), and a DAPI photograph corresponding to the FISH picture is shown on the right side (ii). Images were captured through the oil objective lens (100×) with a CCD camera (SenSys 0400-GI; Photometrics Ltd, Tucson, AZ). Subsequent image processing was performed with the Software IPLab version 2.4.0 (BD Biosciences Bioimaging, Rockville, MD).

using Tetra color one assay kit (Seikagaku Kogyo, Tokyo, Japan). Each experiment was performed 3 times, and typical results are shown.

Results

Identification of a common hemizygous deletion in 10p11 in ATLL by mapping chromosomal breakpoints

We recently studied recurrent chromosomal rearrangements in adult T-cell leukemia lymphoma (ATLL) cells from 61 patients by spectral karyotyping (T.H. et al, manuscript in preparation). In examining the molecular changes in ATLL cells, 605 chromosomal breakpoints in 61 cases were identified and precisely mapped by DAPI banding analysis. The frequency of the breakpoints was counted in each region of the chromosomes, with an average of around 10 translocations in each case (Figure 1A). Most of the chromosomal translocations were unbalanced, and a few recurrent reciprocal translocations were found. Chromosomal breakages were most frequently identified at 10p11 (21 [34.6%] of 61 cases), and they were also frequently represented at 14q11 and 14q32 regions (Figure 1A). Based on the data of SKY, these 3 events occurred almost independently; however, almost 50% of the cases with 14q32 abnormality demonstrated a 10p11.2 abnormality, suggesting that both events are interrelated chromosomal abnormalities. The 10p11 regions were translocated to more than 10 different partner chromosomal regions, such as 21q22, 13q14, and 14q32.

Therefore, we precisely mapped the chromosomal breakpoints at 10p11 in 3 ATLL cell lines (KK1, KOB, and SO4) and 2 primary ATLL cases (ATL018 and ATL090) by FISH. We identified der(10)t(10,22)(p11.2;q13.1) in KK1, der(10)t(10,14)(p11.2;q11.2)

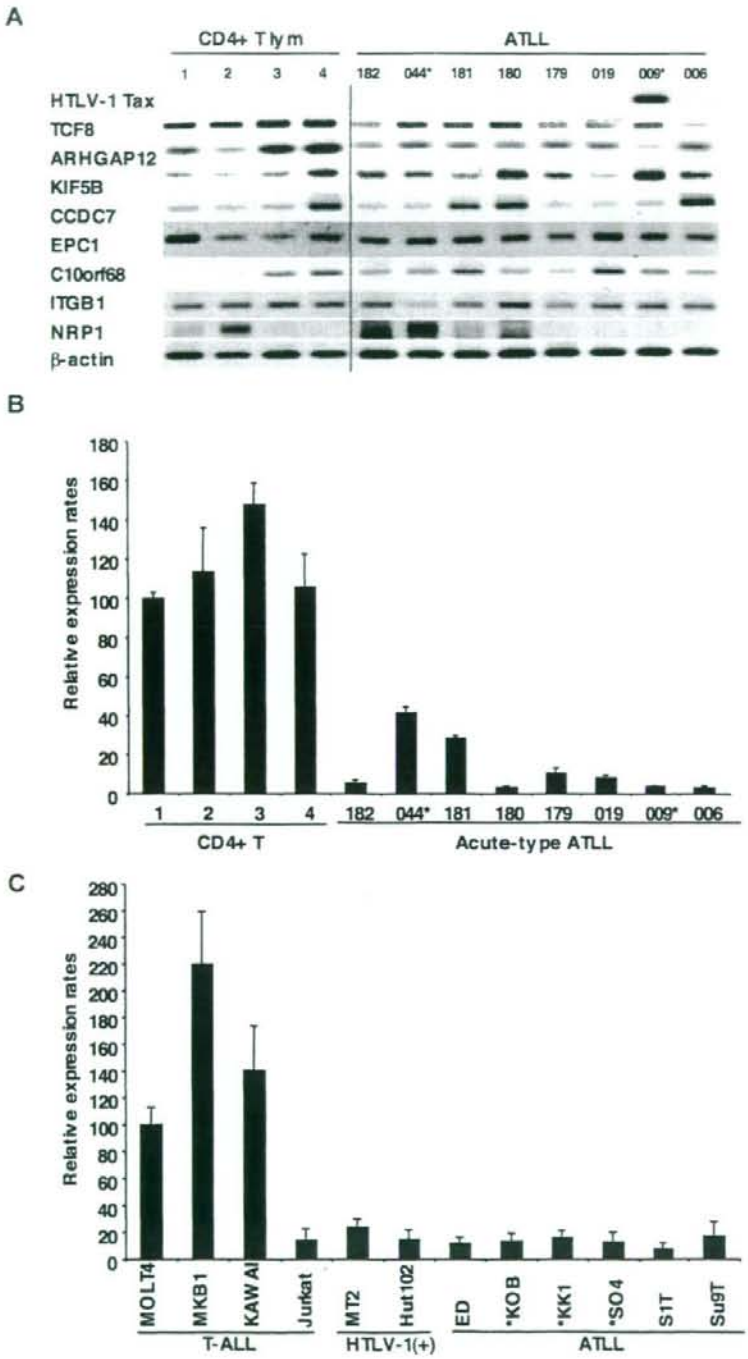

Figure 2. Down-regulated expression of *TCF8* in ATLL cells. (A) The expression profiles of the genes mapped within the deletion region at 10p11. Semiquantitative reverse-transcription PCR (RT-PCR) was performed to determine the expression of the genes mapped within the deletion region. *TCF8, ARHGAP12, KIF5B, CCDC7, EPC1, C10orf68, ITGB1,* and *NRP1* showed a single band of amplified cDNA from $CD4^+$ T lymphocytes from healthy volunteers as controls and from ATLL cells from the patients. A band of HTLV1 *Tax* was amplified from only 1 of 8 ATLL cells. A vertical line has been inserted to indicate a repositioned gel lane. (B) Quantitative RT-PCR analysis of *TCF8* mRNA in 4 samples of $CD4^+$ T lymphocytes from healthy volunteers and 8 samples of ATLL cells from the patients. The data were normalized to *β-actin* mRNA and calibrated to the *TCF8/β-actin* ratio (ΔCT) in the case of healthy volunteer no. 1, as a relative expression rate of 100. The data are the mean and standard deviation of $2^{-\Delta\Delta CT}$ in a duplicate assay. Two patients (indicated by *) have the chromosome 10p11.2 abnormalities. (C) Quantitative RT-PCR analysis of *TCF8* mRNA in various types of T lymphoblastic leukemia cell lines. MOLT4, MKB1, KAWAI, and Jurkat are T-lymphoid leukemia cell lines; MT2 and HUT102 are HTLV-1–infected cell lines; and ED, KOB, KK1, SO4, S1T, and Su9T are ATLL cell lines. Three ATLL cell lines (indicated by *) showed the deletion of chromosome 10p11.2 with *TCF8*.

in KOB, der(10)t(2,10)(p23;p11.2) in SO4, t(10;21)(p11.2;q11.2) in ATL018, and t(10;13)(p11.2;q14) in ATL090 (Table S1, available on the *Blood* website; see the Supplemental Materials link at the top of the online article). Using 53 BAC clones on 10p as DNA probes for FISH (Table S2), the chromosomal breakpoints in these 5 cases were mapped to a 1-Mb region at 10p11.2 (Figure 1B). It was noted that the genomic deletions surrounding the chromosomal breakpoints were detected by a FISH analysis (Figure 1C) and heterozygous deletions of the 10p11.2 region with translocations were found in all 5 samples (Table S2; Figure 1B). Heterozygous deletions of approximately 2 to 8 Mb in the 10p11.2 region with translocations were found in all 5 samples. In addition, no FISH

Table 1. Summary of the genetic and epigenetic abnormalities in ATLL cell lines

Cell line	Cell type	10p abnormalities	Point mutation	Treatment		
				5-Aza-dC, fold ± SD	TSA, fold ± SD	5-Aza-dC + TSA, fold ± SD
MOLT4	T-ALL	None	None	1.25 ± 0.46	1.65 ± 0.21	1.65 ± 0.22
Jurkat	T-ALL	None	None	11.17 ± 0.59*	10.04 ± 1.74*	3.07 ± 0.54*
MT2	HTLV-1 (+)	None	None	3.38 ± 1.17*	8.25 ± 1.76*	4.58 ± 0.90*
HUT102	HTLV-1 (+)	None	255A>C Asn78Thr	4.39 ± 0.49*	6.94 ± 0.16*	8.03 ± 1.05*
ED	ATLL	None	None	4.32 ± 1.57*	7.48 ± 0.91*	3.93 ± 0.21*
KOB	ATLL	10p del	None	3.26 ± 1.12*	2.32 ± 0.81	2.08 ± 0.54
KK1	ATLL	10p del	None	9.92 ± 0.45*	6.76 ± 0.17*	9.72 ± 0.35*
SO4	ATLL	10p del	None	1.40 ± 0.33	1.57 ± 0.18	0.59 ± 0.06
S1T	ATLL	None	None	3.66 ± 0.21*	3.95 ± 0.75*	2.32 ± 1.63
Su9T	ATLL	None	None	3.91 ± 0.45*	9.66 ± 2.38*	1.42 ± 0.21

Data are means plus or minus SD.
*$P < .05$ versus control (Dunnett test).

signals were detected in the 1-Mb region from RP11-135A24 to RP11-462L8 in ATL090, suggesting that a 10p11 region-specific homozygous deletion had occurred in this case (Figure 1B). Therefore, a minimal common region of chromosome deletions, including a region of homozygous deletion in ATL090, was mapped to a 2-Mb region from PR11-523J14 to RP11-342D11 (Figure 1B).

To confirm these results, we performed SNP array-CGH using DNA from 8 ATLL-related cell lines including KK1, KOB, SO4, and an additional 10 samples from acute-type ATLL patients. Deletions in 10p11.2, including the 2-Mb deletion region, were noted in 3 cell lines: KK1, KOB, and SO4, and an additional 4 patient samples (Figure 1B; Table S3). Using SNP array-CGH, the telomeric deleted regions in chromosome 10p11.2 in KOB and KK1 covered a wider area than those detected by FISH analysis, and each deleted region in the 3 cell lines and 4 patients samples covered the common deletion region. To combine these data, the same minimal common region of chromosome deletions, including regions of homozygous deletion in ATL090, was mapped to a 2-Mb region from PR11-523J14 to RP11-342D11 (Figure 1B), suggesting that a tumor suppressor gene possibly exists in this 2-Mb region in 10p11.2.

Down-regulation of *TCF8* mRNA in ATLL cells

We examined the mRNA expression profiles of all 12 genes within the commonly deleted region in 10p11.2, which were identified by NCBI and Celera gene maps (Rockville, MD). Since mRNA samples from the ATLL patients used for the deletion mapping were not available, we initially used the mRNA expression profiles of the other 8 leukemia cell samples from acute-type ATLL patients by semiquantitative reverse-transcription PCR (RT-PCR), which had been previously identified by DNA microarray.[15] Two leukemia samples from patients with ATLL had chromosome 10p11.2 abnormalities: t(10;15) (p11.2;q26) in ATL044 and monosomy 10 in ATL009 (Table S1). Expression levels of 8 genes (*TCF8, ARHGAP12, KIF5B, CCDC7, EPC1, C10orf68, ITGB1* and *NRP1*) and HTLV-1 *Tax* as well as *β-actin* are shown in Figure 2A. The results showed that levels of *TCF8* mRNA in ATLL cells had a tendency to be lower than those in $CD4^+$ T lymphocytes from healthy volunteers, even though only 2 of 8 patients had chromosome 10p11.2 abnormalities. Other genes did not show any differences in expression level between the 2 groups. Expression profiles of the leukemia cells using a DNA microarray gave the same results (Figure S1), and quantitative real-time RT-PCR also showed that the expression level of *TCF8* mRNA in ATLL cells was significantly lower than that in $CD4^+$ T lymphocytes (Figure 2B).

To confirm these results, 12 T-ALL cell lines containing 6 ATLL cell lines (ED, KOB, KK1, SO4, S1T, and Su9T), 2 HTLV-1–infected T-cell lines (MT2 and HUT102), and 4 HTLV-1–uninfected T-ALL cell lines (Jurkat, MOLT4, MKB1, and KAWAI) were used for an expression study. Three cell lines (KOB, KK1, and SO4) revealed the deletion of chromosome 10p11.2 with *TCF8*. Although no other genes except *TCF8* showed any change in expression level in these cell lines (Figure S2), the expression level of *TCF8* was specifically down-regulated in all of the ATLL cell lines along with Jurkat cells by quantitative real-time RT-PCR (Figure 2C). These data suggest that *TCF8* transcription might be down-regulated by epigenetic inactivation in most ATLL-related cell lines with Jurkat cells.

Increased expression of *TCF8* by 5-aza-2′-deoxycytidine or trichostatin A in ATLL cell lines

To clarify whether DNA methylation and/or histone deacetylation of the *TCF8* gene promoter were involved in the transcriptional repression of *TCF8* in ATLL cell lines with Jurkat cells, 10 cell lines (2 T-ALL, 2 HTLV-1–infected, and 6 ATLL-derived cell lines) were cultured with (1) 10 μM 5-aza-2′-deoxycytidine (5-aza-dC), a DNA demethylating agent, for 72 hours, (2) 1.2 μM trichostatin A (TSA), an inhibitor of histone deacetylase, for 48 hours, or (3) 1.2 μM TSA for 48 hours following culture with 10 μM 5-aza-dC for 24 hours. After treatment with 5-aza-dC, *TCF8* expression was up-regulated in 8 of 10 cell lines (Jurkat, MT2, HUT102, ED, KOB, KK1, S1T, and Su9T), with more than 3-fold activation ($P < .05$) as detected by real-time RT-PCR (Table 1). After treatment with TSA for 48 hours, the levels of *TCF8* mRNA increased in 7 of 10 cell lines (Jurkat, MT2, HUT102, ED, KK1, S1T, and Su9T), also with more than 3-fold activation ($P < .05$). In addition, combination therapy induced *TCF8* mRNA expression in 5 cell lines by more than 3-fold. Therefore, *TCF8* mRNA expression was activated in 7 of 8 ATLL-related cell lines along with Jurkat cells by either 5-aza-dC or TSA treatment, suggesting that the down-regulation of *TCF8* in most of the ATLL cell lines except SO4 cells with a chromosome 10p hemizygous deletion was dependent on epigenetic abnormalities.

Unmethylated putative *TCF8* promoter in ATLL cell lines

Next, we determined the methylation status of the *TCF8* promoter by bisulfite sequencing. A CpG island containing 50 CpGs was

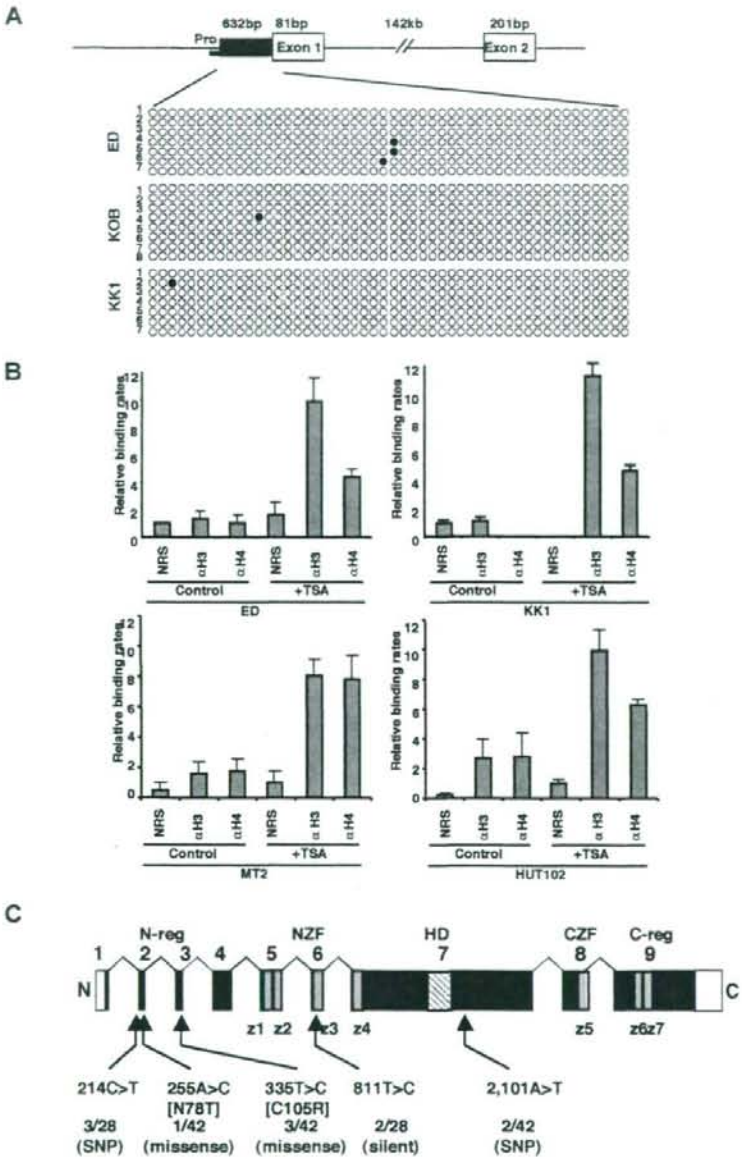

Figure 3. Genetic and epigenetic abnormalities of the *TCF8* gene in ATLL cells. (A) Bisulfite genomic sequencing of the *TCF8* promoter region in 3 ATLL cell lines: ED, KOB, and KK1. PCR products amplified from bisulfite-treated DNA were subcloned, and 8 clones in each cell line were sequenced. ○ indicate unmethylated CpGs (Thy), and ● indicate methylated CpGs (Cyt). The sequenced region contains 50 CpGs in 632 bp, just upstream from exon 1. Pro indicates a region of the *TCF8* promoter for chromatin immunoprecipitation. (B) Specific DNA binding of acetylated histone H3 or H4 to the *TCF8* promoter region detected by chromatin immunoprecipitation (ChIP). Two genomic DNA fragments containing every possible DNA-binding site, *TCF8* promoter, or *β-actin* promoter were amplified from the genomic DNA of fixed ATLL-related cell lines (MT2, HUT102, ED, and KK1) after immunoprecipitation with normal rabbit serum (NRS) or with antiacetylated histone H3 or H4 antibodies (αH3 or αH4). Quantitative PCR data calibrated to the *TCF8* promoter/*β-actin* ratio are shown in the NRS as a relative expression rate of 1. Data are the means plus or minus standard deviation of $2^{-\Delta\Delta Ct}$ in a duplicate assay. Cell lines were cultured in RPMI1640 medium containing 10% FCS with (+ TSA) or without (control) 1.2 μM TSA. (C) Genomic structure of the *TCF8* gene with a missense mutation and single nucleotide polymorphisms. Locations of the mutations and the single nucleotide polymorphisms relative to the exons encoding the functional domains are shown. *TCF8* encodes a homeodomain (HD) flanked by 2 zinc-finger clusters (z1 to z4 and z5 to z7) (NZF indicates N-terminal zinc finger repeats, CZF; C-terminal zinc finger repeats). The N-terminal transcriptional regulatory domain (N-reg) could bind to p300/CBP and the C-terminal transcriptional regulator domain (C-reg) is the region where acidic amino acids are clustered just after the last zinc-finger domain. Values represent the number of mutated cases per total number of tested cases. SNP indicates single nucleotide polymorphism. White boxes represent noncoding regions in exons 1 and 9.

amplified from a 632-bp region of the putative *TCF8* promoter adjacent to exon 1 using 2 pairs of PCR primers and bisulfite-treated genomic DNA from 3 ATLL cell lines: ED, KOB, and KK1. However, the *TCF8* promoter was not methylated in any of the 3 ATLL cell lines in which *TCF8* expression was induced by 5-aza-dC (Figure 3A), suggesting that the CpG island was not a direct target for DNA methylation in ATLL cells. Moreover, *TCF8* mRNA was up-regulated in various ATLL cell lines after treatment with hydralazine, which was reported to decrease DNA methyltransferase expression (Figure S3). This observation suggests that a transactivating regulator of *TCF8* may be modulated by methylation or the other regulatory elements are located outside the *TCF8* promoter. Such enhancer-related methylation events have been described for the imprinting of *H19* and *Igf2*, *p21WAF1* regulation by *p73*, and *Apaf-1*.[30-33] Therefore, further analyses will be needed to determine the exact regulatory element near the *TCF8* gene or to find a transactivating regulator of *TCF8*, which is directly methylated in ATLL cells.

Histone deacetylation is directly involved in down-regulation of *TCF8* mRNA expression in ATLL cells

To confirm the correlation between reduced *TCF8* mRNA expression and histone deacetylation, *TCF8* expression and histone acetylation status were analyzed in the ATLL-related cell lines (MT2, HUT102, ED, and KK1) by chromatin immunoprecipitation (ChIP) after treatment with or without TSA. After treatment with TSA for 48 hours, the chromosomal DNA precipitated by antiacetylated histone H3 or H4

antibody was amplified with 2 sets of primers for the *TCF8* promoter region or for the human *β-actin* promoter region (Figure 3B). Band intensities of the *TCF8* promoter region in 4 cell lines were amplified 3- to 6-fold after treatment with TSA, indicating that histone deacetylation of the *TCF8* promoter region was directly involved in the down-regulation of *TCF8* mRNA expression in ATLL cells.

Identification of missense mutations in *TCF8* in ATLL cells

We then searched for somatic *TCF8* mutations in DNA samples from 34 patients with acute-type ATLL and 10 T-cell leukemia cell lines. Genomic PCR did not detect any homozygous deletions in any of the 9 coding exons of *TCF8* in these samples. We detected 5 types of nucleotide substitutions, and all were heterozygous (Figure 3C). The 255A>C substitution in HUT102, creating a missense mutation (Asn78Thr) in exon 2, and the 335T>C substitution in the leukemia cells from 3 ATLL patients, creating a missense mutation (Cys105Arg) in exon 3, were likely to be somatic mutations (Table S4), since they were not detected in noncancerous cells from 95 Japanese volunteers.

The results of genomic and expression analysis indicate that the *TCF8* gene is altered by several mechanisms, including hemizygous deletion, epigenetic dysregulation, and intragenic mutations. Regarding the ATLL-related cell lines, 3 of 9 showed hemizygous deletions of 10p11.2; 8 of 9 showed epigenetic dysregulation of the *TCF8* gene; and 1 of 9 showed an intragenic mutation (Table 1). Therefore, *TCF8* is a strong candidate tumor suppressor gene for ATLL leukemogenesis and is initially inactivated by unbalanced translocations with heterozygous deletion in the 10p11.2 region in ATLL cells.

Development of CD4+ T-cell lymphoma in *TCF8* mutant mice

To determine whether down-regulation of the *TCF8* gene could be a causative event for leukemogenic conversion of T lymphocytes to leukemia-lymphoma cells, we investigated δ*EF1* (mouse homologue of *TCF8*) gene-targeted mutant mice, which lack the COOH-proximal zinc finger clusters (δ$EF1^{\Delta C/\Delta C}$ allele) and were reported to have a defect in the thymic T-cell development.[28,29] Since 20% of the homozygous *TCF8* mutant mice were born alive, we made their genetic backgrounds more heterogeneous by crossing the C57BL/6 background with the ICR or F1 (C57BL/6 × C3H) mice. Homozygous mice on a mixed genetic background were born with almost normal Mendelian frequencies (wild-type: heterozygote:homozygote = 60:91:42). After 4 months, almost half of the *TCF8* homozygous mutant mice experienced enlargement of the abdomen due to ascites (27 [64.3%] of 42 mice), and many mice developed lymphomas with a median onset of disease of 30 weeks after birth and an earliest onset at 95 days after birth (Figure 4A). Half of the mice died within a year, and 84% of them developed fatal T-cell lymphomas. In *TCF8* homozygous mutant mice, 2 types of lymphomas were observed: (1) peripheral lymphomas with or without ascites, and (2) thymic tumors. Typical pathological findings of 15 mice (no. 6 to no. 21) are shown in Table S5. In the peripheral lymphoma group, a large amount of bloody or milky ascitic fluid had collected in approximately 60% of the mice with invasion of various organs (Figure 4B,C). Numerous lymphoma cells with medium to large, cleaved or noncleaved nuclei were observed in the ascitic fluid (Figure 4D). Lymphoma cells had invaded various lymph nodes, including the thoracic, peripancreatic, mesenteric, perirenal, mesenteric, and other peripheral lymph nodes (Figure 4E). Fluorescence-activated cell sorter

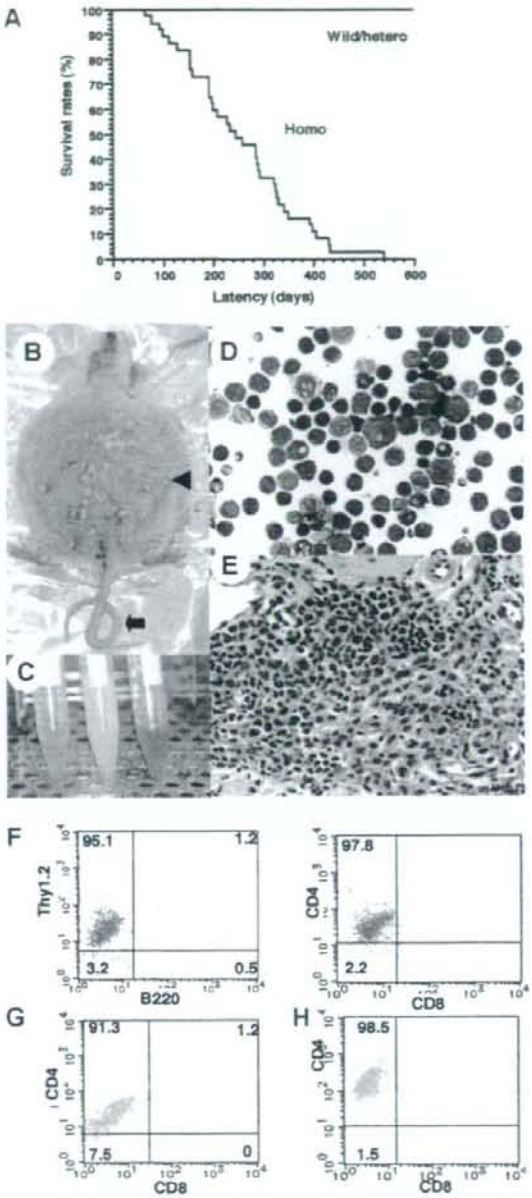

Figure 4. Survival rates and pathologic findings in *TCF8* mutant mice. (A) The survival rates of a cohort of wild-type (wild), *TCF8* heterozygous (hetero), and *TCF8* homozygous (homo) mutant mice were followed over the indicated period using Kaplan-Meier plots. (B) Gross photograph of *TCF8* mutant mice with ascites (◀). Approximately 30% of *TCF8*-homologous mutant mice showed curled tail (◖). (C) Bloody or milky ascites was pooled. (D) May-Giemsa staining of tumor cells in ascites. Original magnification ×400. (E) Many lymphoma cells with medium- to large-sized nuclei infiltrated in the mesentery. Cells were examined using an Axioskop 2 plus inverted microscope (Carl Zeiss, Rugby, United Kingdom) and digital images were aquired using AxioCam camera and AxioVision 2.05 software (Carl Zeiss). Original magnification ×400. (F) Tumor cells from ascitic fluids were analyzed by staining with a combination of monoclonal antibodies, either Thy1.2-PE with B220-FITC (left) or CD4-PE with CD8-FITC (right) and FACS. (G,H) The tumor cells that invaded liver (G) or spleen (H) were analyzed by staining with a combination of monoclonal antibodies, CD4-PE with CD8-FITC.

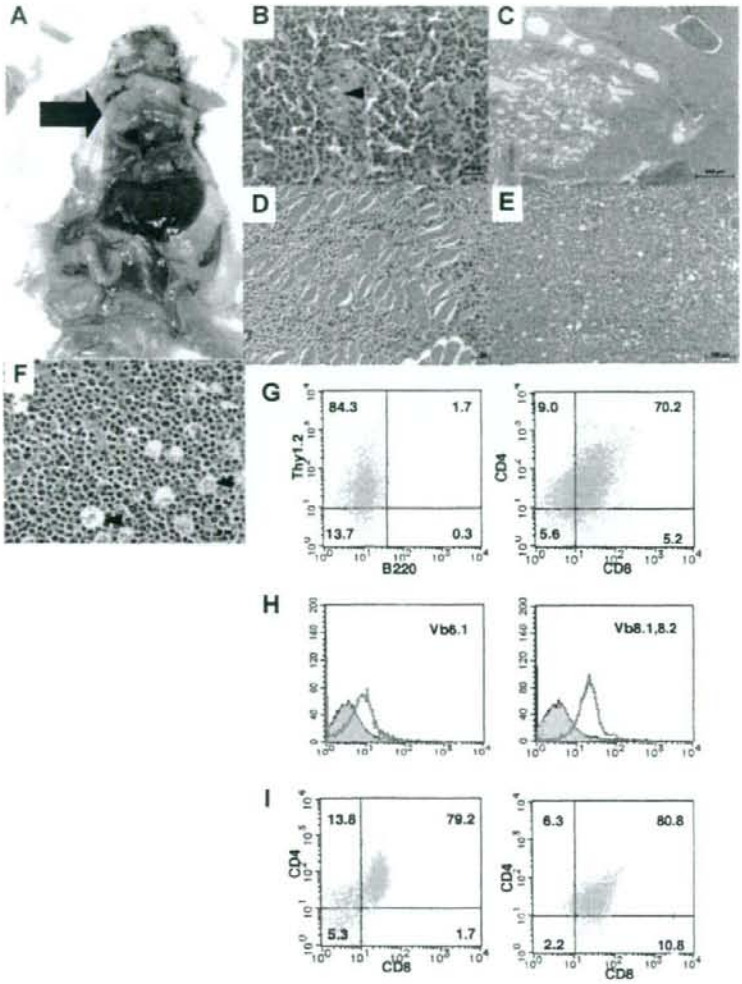

Figure 5. Pathological findings of *TCF8* mutant mice. (A) Gross autopsy of *TCF8* mutant mice with thymic tumors. A large thymic tumor (➡) was observed at the mediastinum of the dissected mouse. (B) Hematoxylin and eosin staining of tumor sections from the mouse as indicated. The normal thymic cellular architecture in the *TCF8* mutant mice is replaced with monotonous fields of large, highly mitotic lymphoblasts with small Hassall bodies (◀). The scale bar indicates 20 μm. Original magnification ×400. (C) The tumor cells invaded the lung, vascular tissues, and heart in the mouse. The scale bar indicates 500 μm. Original magnification ×25. (D) The tumor cells invaded the muscular tissues of the chest wall. The scale bar indicates 50 μm. Original magnification ×200. (E) Hematoxylin and eosin staining of peripheral lymph nodes. Tumor cells showed a diffuse proliferation of monomorphic lymphoma cells, focally mixed with tingible body macrophages ("starry-sky appearance") (◀). The scale bar indicates 100 μm. Original magnification ×100. (F) Hematoxylin and eosin staining of peripheral lymph nodes. The scale bar indicates 20 μm. Original magnification ×400. (G) Tumor cells from the thymic tumor were analyzed by staining with a combination of monoclonal antibodies, either Thy1.2-PE with B220-FITC (left) or CD4-PE with CD8-FITC (right) and FACS. (H) The tumor cells of the $CD3^+B220^-$ population did not express Vβ6.1 TCR (left), but showed weak expression of Vβ8.1-8.2 TCR (right). (I) Tumor cells from the liver (left) or spleen (right) were analyzed by staining with a combination of monoclonal antibodies, CD4-PE and CD8-FITC.

(FACS) analysis of the tumor cells showed that most of the lymphoma cells in the ascitic fluid and those that had invaded various organs were $CD4^+$ SP T cells (Figure 4F-H).

In the thymic tumor group, 16% of the homozygous mutant mice had large thymic tumors with a diameter of 1 to 3 cm (Figure 5A). Histologic analysis of the thymic tumors revealed that lymphoblastic lymphoma cells had densely proliferated in the cortex and medulla of the thymus (Figure 5B). Thymic lymphoma cells continuously invaded the lungs, chest wall, and pericardium (Figure 5C,D). In the peripheral lymph nodes, there was diffuse proliferation of monomorphic lymphoma cells focally mixed with tingible body macrophages, giving a "starry-sky" appearance (Figure 5E,F). In the thymic tumor group, surface marker analysis of thymic lymphoma cells revealed $CD4^+CD8^+$ DP T lymphoma cells (Figure 5G), which were negative for Vβ6.1 TCR and weakly positive for Vβ8.1-8.2 TCR with a single peak (Figure 5H). In this mouse, the mononuclear cells that invaded the liver, as well as a majority of the cells that invaded the spleen, were DP T lymphoma cells (Figure 5I). Therefore, in the same mouse, both tumor cells derived from the thymus and those that had invaded the organs were revealed to be DP T lymphoma cells. Moreover, the remaining mice with large thymic tumors showed the same $CD4^+CD8^+$ DP T lymphoma cells. In total, 84% of the T-cell tumors in *TCF8* homologous mutant mice could be classified as $CD4^+$ SP T-cell lymphoma, and 16%, as $CD4^+CD8^+$ DP thymic T-cell lymphoma. $CD8^+$ SP T lymphomas were never observed. Thus, the histopathological and cellular findings revealed that $CD4^+$ T-cell lymphoma/leukemia developed in most *TCF8* mutant mice.

Down-regulation of TCF8 expression is associated with TGF-β1 resistance in ATLL cells

The TGF-β superfamily is known to inhibit the lineage commitment of double-positive (DP) cells toward $CD4^+$ T-cell differentiation.[34] Interestingly, the ATLL cells were found to be resistant to growth inhibition by TGF-β1, even with high levels of TGF-β1 expression,[35-37] suggesting that ATLL cells may have developed several mechanisms of resistance to escape the antiproliferative and inactivating signal mediated by TGF-β1, including Tax through activation of the JNK/c-Jun pathway[38,39] or MEL1S expression.[37] Since TCF8 is reported to synergize with Smad

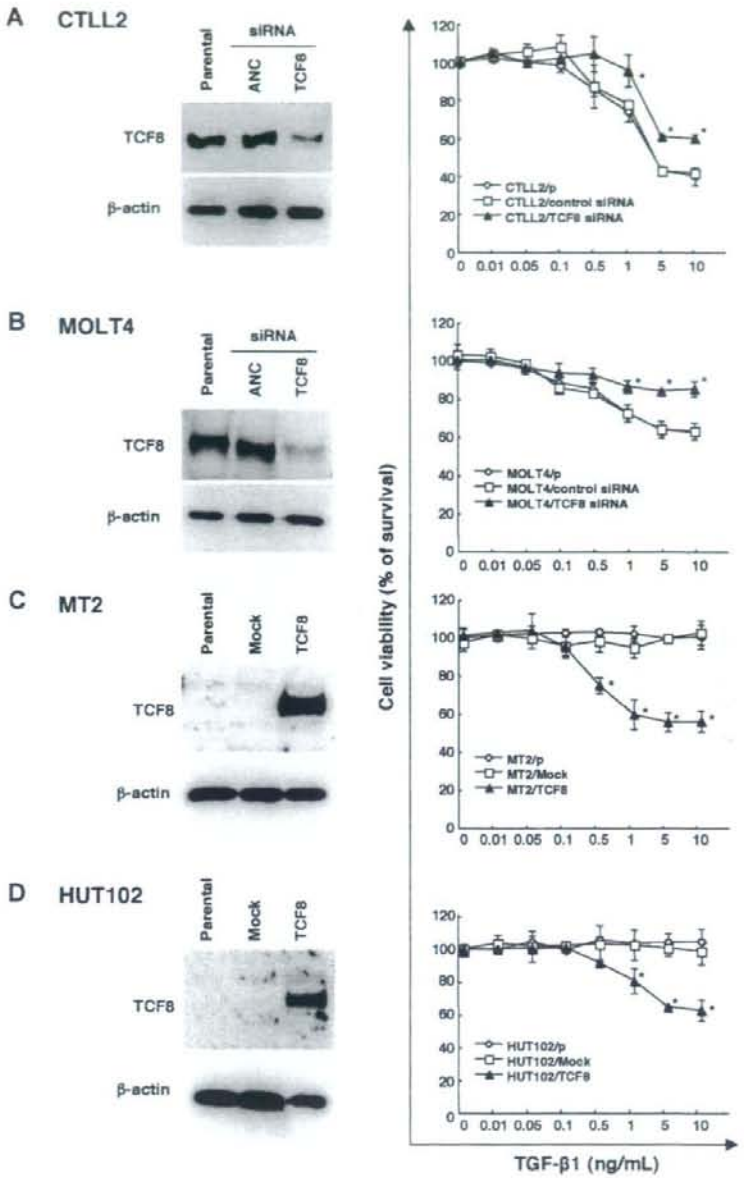

Figure 6. TGF-β1 responsiveness in various leukemia cell lines with the up- or down-regulation of TCF8 expression. (A,B) The down-regulation of the TCF8 protein by *TCF8* siRNA. The CTLL2 (A) and MOLT4 (B) cell lines were transfected with either *TCF8* or the AllStars Negative Control (ANC) siRNAs and then were incubated for 24 hours. The levels of TCF8 protein were examined in each cell line by Western blotting (left panel). After transfection with siRNAs, the cells were treated with the indicated concentrations of TGF-β1 for 72 hours. The degree of proliferation of each cell line was examined by MTT assay. The results are shown as percentages of the values obtained from the control TGF-β1–free culture (right panel). A ◇ represents parental cells, □ represents cells treated with ANC siRNA, and ▲ represents cells treated with *TCF8* siRNA. Student *t* test ($P < .05$) was used for the statistical analysis. (C,D) The enforced expression of TCF8 in HTLV-1–infected cell lines. The TCF8 protein levels were examined in each MT-2 (C) and HUT102 (D) cell transfected with a mock or TCF8 expression plasmid after 24 hours by Western blotting (left panel). The cells were treated with the indicated concentrations of TGF-β1 for 72 hours and the proliferation of each was examined by MTT assay. The results are shown as percentages of the values obtained from the control TGF-β1–free culture (right panel). Parental cells (◇), mock vector-transfected cells (□), and TCF8 expression plasmid-transfected cells (▲). All data are the means plus or minus standard deviation in a duplicate assay. Student *t* test ($P < .05$) was used for the statistical analysis.

proteins to activate TGF-β1 signal transduction,[40,41] we investigated whether the down-regulation of TCF8 expression was associated with resistance to TGF-β1–mediated growth inhibition in ATLL cells. Thereafter, either *TCF8* or ANC siRNA was introduced into a murine IL2–dependent T-lymphoma cell line, CTLL2, and human T-ALL cell line, MOLT4. Western blot analyses revealed the TCF8 expression in the siRNA-treated cells to be less than half of that in the control cells, while the viable cell curves of both cell lines treated with *TCF8* siRNA exhibited a significantly higher resistance to TGF-β1 than those of the control cells (Figure 6A,B). Next, the TCF8 expression plasmid was transiently introduced into 2 HTLV-1–infected T-cell lines (MT2 and HUT102) and up to 40% of the TCF8 transfectants died after TGF-β1 treatment in a dose-dependent manner, whereas the parental and transfectants with mock plasmid did not die with TGF-β1 treatment at all (Figure 6C,D). These results indicate that down-regulation of TCF8 expression is one of the mechanisms of TGF-β1 resistance in ATLL cells, suggesting that $CD4^+$ T lymphoma cells might escape from negative selection due to reduced TGF-β1 responsiveness.

Discussion

We demonstrated that in ATLL cells, the *TCF8* gene was mainly epigenetically inactivated in a majority of ATLL cells. In addition,

TCF8 (or $\delta EF1^{\Delta C\text{-}fm}$ homozygous) mutant mice frequently developed CD4+ T-cell lymphoma and/or leukemia after a few months. These findings indicate that *TCF8* has a tumor suppressor role in ATLL. Since the heterozygous *TCF8* mutant mice did not develop any tumors and the level of TCF8 expression in some ATLL cells was approximately 30% to 40% of that observed in the control CD4 lymphocytes, TCF8 may therefore be involved in only some and not all of ATLL development. On the other hand, it is reported that *TCF8* overexpressed in colorectal or breast cancer cells induces epithelial-mesenchymal transition (EMT) with the development of metastatic properties such as migration and invasion in vitro and in vivo.[42] Therefore, *TCF8* has dual functions in cancer progression, which are dependent on the type of the tumors, such as *WT1* or *TSLC1* tumor suppressor genes.[43,44]

It was previously reported that *TCF8* mutant mice had a defect in T-cell development in the first week of life.[28] At the early stage of development, intrathymic c-kit+ T precursor cells in these mice were depleted to just 1% of the level in normal mice, and the number of CD8+ SP T cells was significantly reduced relative to the number of CD4+ SP T cells. These observations indicate that TCF8 is involved in the regulation of T-cell development at multiple stages. Lymphoma cells in *TCF8* mutant mice showed either CD4+ SP T cells or DP T cells after 6 months. Interestingly, TGF-β1 was important for regulating T-cell development in the thymus and for negative selection at the late stage of differentiation of DP T cells to CD4+ SP cells.[34] Recently, DNA microarray analysis identified a higher level of *TCF8* expression in DP thymocytes to CD4+ SP T cells,[45] suggesting that TCF8 enhanced negative selection due to TGF-β1 responsiveness. Moreover, *TGF-β1*–deficient mice had an increased number of CD4+ SP T cells and a decreased number of CD8+ SP T cells.[46,47] By correlating the development of CD4+ SP T-lymphoma cells in *TCF8* mutant mice with the increase in the number of CD4+ T cells in *TGF-β1*–deficient mice, we concluded that leukemogenesis in *TCF8* mutant mice was partly dependent on resistance to TGF-β1.

TCF8 is an E-box–binding transcription factor reported to regulate many genes. We found that the transcription of *CD4*, *α4 integrin*, and *GATA-3*, which was reported to be suppressed by TCF8,[48] was up-regulated in ATLL cells (data not shown). It was therefore suggested that impaired regulation of TCF8 expression in ATLL induced the increase in expression of *CD4* and *GATA3*, which was crucial for the establishment of the ATLL phenotype in CD4+ SP helper T lymphocytes. Moreover, TCF8 was reported to regulate p73, CCNG2, or p130.[49,50] Since these genes are very important for cell-cycle progression and apoptosis, further investigation is needed to determine which ones are directly related to leukemogenesis among those regulated by TCF8.

The phenotypes of T-cell lymphomas in *TCF8* mutant mice were very similar to those of ATLL patients. In *TCF8* mutant mice, the tumor cells were mainly CD4+ SP or DP T cells, which invaded various organs, such as the liver, spleen, and lungs. In ATLL, the tumor cells were mainly CD4+ SP T cells that also invaded various organs. One difference, however, was that thymic lymphomas developed in the *TCF8* mutant mice, which has not been reported in ATLL cases. Another difference is that lymphoma cells in *TCF8* mutant mice did not have multilobulated nuclei. Such nuclei result from alterations in the PI3-kinase signaling cascades,[51] suggesting that down-regulation of TCF8 expression is not related to the PTEN signaling pathway and that other mutations are necessary for the development of ATLL. This is the first report illustrating the importance of the disruption of *TCF8* in leukemogenesis of ATLL.

Acknowledgments

We thank Drs M. Shiraga, I. Nishikata, and T. Uetsuki for technical assistance and advice on the paper.

This work was supported by Grants-in-Aid for Scientific Research of Priority Area and for 21st Century COE program (Life science) from the Ministry of Education, Culture, Sports, Science and Technology, Japan Leukemia Research fund, and Research fund from Miyazaki Prefecture Collaboration of Regional Entities for the Advancement of Technological Excellence, Japan Science and Technology Corporation.

Authorship

Contribution: T.H., S.N., and K.H. designed and performed experiments, analyzed data, and drafted the paper; M.H. performed experiments; T.K., Y.A., T.T., K.N., and M.T. performed experiments and data analysis; Y.A. and R.Y. performed the histopathology; K.Y., A.O., and H.T. collected case material and supervised the project; J.Y. and Y.H. supervised the project and drafted the paper; K.M. designed the experiments, analyzed data, and drafted the paper.

Conflict-of-interest disclosure: The authors declare no competing financial interests.

Correspondence: Kazuhiro Morishita, Division of Tumor and Cellular Biochemistry, Department of Medical Sciences, Faculty of Medicine, University of Miyazaki, 5200 Kihara, Kiyotake, Miyazaki, Japan, 889-1692; e-mail: kmorishi@med.miyazaki-u.ac.jp.

References

1. Takatsuki K, Yamaguchi K, Kawano F, et al. Clinical diversity in adult T-cell leukemia-lymphoma. Cancer Res. 1985;45:4644s-4645s.
2. Matsuoka M. Human T-cell leukemia virus type I and adult T-cell leukemia. Oncogene. 2003;22:5131-5140.
3. Yoshida M. Multiple viral strategies of HTLV-1 for dysregulation of cell growth control. Annu Rev Immunol. 2001;19:475-496.
4. Tamiya S, Matsuoka M, Etoh K. Two types of defective human T-lymphotropic virus type I provirus in adult T-cell leukemia. Blood. 1996;88:3065-3073.
5. Koiwa T, Hamano-Usami A, Ishida T. 5'-long terminal repeat-selective CpG methylation of latent human T-cell leukemia virus type 1 provirus in vitro and in vivo. J Virol. 2002;76:9389-9397.
6. Okamoto T, Ohno Y, Tsugane S, et al. Multi-step carcinogenesis model for adult T-cell leukemia. Jpn J Cancer Res. 1989;80:191-195.
7. Look AT. Oncogenic transcription factors in the human acute leukemias. Science. 1997;278:1059-1064.
8. Kamada N, Sakurai M, Miyamoto K, et al. Chromosome abnormalities in adult T-cell leukemia/lymphoma: a karyotype review committee report. Cancer Res. 1992;52:1481-1493.
9. Tsukasaki K, Krebs J, Nagai K, et al. Comparative genomic hybridization analysis in adult T-cell leukemia/lymphoma: correlation with clinical course. Blood. 2001;97:3875-3881.
10. Oshiro A, Tagawa H, Ohshima K, et al. Identification of subtype-specific genomic alterations in aggressive adult T-cell leukemia/lymphoma. Blood. 2006;107:4500-4507.
11. National Center for Biotechnology Information. GenBank. http://www.ncbi.nlm.nih.gov/site/entrez. Accessed December 12, 2007.
12. Williams TM, Moolten D, Burlein J, et al. Identification of a zinc finger protein that inhibits IL-2 gene expression. Science. 1991;25:1791-1794.
13. Barrallo-Gimeno A, Nieto MA. The Snail genes as inducers of cell movement and survival: implications in development and cancer. Development. 2005;132:3151-3161.
14. Thiery JP, Sleeman JP. Complex networks orchestrate epithelial-mesenchymal transitions. Nat Rev Mol Cell Biol. 2006;7:131-142.
15. Sasaki H, Nishikata I, Shiraga T, et al. Overexpression of a cell adhesion molecule, TSLC1, as

a possible molecular marker for acute-type adult T-cell leukemia. Blood. 2005;105:1204-1213.

16. Shimoyama M. Diagnostic criteria and classification of clinical subtypes of adult T-cell leukaemia-lymphoma: a report from the Lymphoma Study Group (1984-87). Br J Haematol. 1991;79:428-437.
17. Schneider U, Schwenk HU, Bornkamm G. Characterization of EBV-genome negative "null" and "T" cell lines derived from children with acute lymphoblastic leukemia and leukemic transformed non-Hodgkin lymphoma. Int J Cancer. 1977;19:621-626.
18. Minowada J, Onuma T, Moore GE. Rosette-forming human lymphoid cell lines. I. Establishment and evidence for origin of thymus-derived lymphocytes. J Natl Cancer Inst. 1972;49:891-895.
19. Yamada Y, Ohmoto Y, Hata T, et al. Features of the cytokines secreted by adult T cell leukemia (ATL) cells. Leuk Lymphoma. 1996;21:443-447.
20. Okada M, Maeda M, Tagaya Y, et al. TCGF (IL 2)-receptor induction Factor (S), II: possible role of ATL-derived factor (ADF) on constitutive IL 2 receptor expression of HTLV-1(+) T cell lines. J Immunol. 1985;135:3995-4003.
21. Miyoshi I, Kubonishi I, Yoshimoto S, et al. Type C virus particles in a cord T-cell line derived by cocultivating normal human cord leukocytes and human leukaemic T cells. Nature. 1981;294:770-771.
22. Gillis S, Smith KA. Long term culture of tumour-specific cytotoxic T cells. Nature. 1977;268:154-156.
23. Shaffer LG, Tommerup N (eds). ISCN (2005): An International System for Human Cytogenetic Nomenclature. S. Karger, Basel; 2005.
24. Kakazu N, Taniwaki M, Horiike S, et al. Combined spectral karyotyping and DAPI banding analysis of chromosome abnormalities in myelodysplastic syndrome. Gene Chromosome Cancer. 1999;26:336-345.
25. Taniwaki M, Nishida K, Ueda Y, et al. Interphase and metaphase detection of the breakpoint of 14q32 translocations in B-cell malignancies by double-color fluorescence in situ hybridization. Blood. 1995;85:3223-3228.
26. National Center for Biotechnology Information. http://www.ncbi.nlm.nih.gov/project/genome. Accessed December 12, 2007.
27. Nannya Y, Sanada M, Nakazaki K, et al. A robust algorithm for copy number detection using high-density oligonucleotide single nucleotide polymorphism genotyping arrays. Cancer Res. 2005;65:6071-6079.
28. Higashi Y, Moribe H, Takagi T, et al. Impairment of T cell development in deltaEF1 mutant mice. J Exp Med. 1997;185:1467-1479.
29. Takagi T, Moribe H, Kondoh H, Higashi Y. DeltaEF1, a zinc finger and homeodomain transcription factor, is required for skeleton patterning in multiple lineages. Development. 1998;125:21-31.
30. Hark AT, Schoenherr CJ, Katz DJ, et al. CTCF mediates methylation-sensitive enhancer-blocking activity at the H19/Igf2 locus. Nature. 2000;405:486-489.
31. Bell AC, Felsenfeld G. Methylation of a CTCF-dependent boundary controls imprinted expression of the Igf2 gene. Nature. 2000;405:482-485.
32. Schmelz K, Wagner M, Dörken B, Tamm I. 5-Aza-2′-deoxycytidine induces p21WAF expression by demethylation of p73 leading to p53-independent apoptosis in myeloid leukemia. Int J Cancer. 2005;114:683-695.
33. Soengas MS, Capodieci P, Polsky D. Inactivation of the apoptosis effector Apaf-1 in malignant melanoma. Nature. 2001;409:207-211.
34. Licona-Limon P, Soldevila G. The role of TGF-beta superfamily during T cell development: new insights. Immunol Lett. 2007;109:1-12.
35. Niitsu Y, Urushizaki Y, Koshida Y, et al. Expression of TGF-beta gene in adult T cell leukemia. Blood. 1988;71:263-266.
36. Kim SJ, Kehrl JH, Burton J, et al. Transactivation of the transforming growth factor beta 1 (TGF-beta 1) gene by human T lymphotropic virus type 1 tax: a potential mechanism for the increased production of TGF-beta 1 in adult T cell leukemia. J Exp Med. 1990;172:121-129.
37. Yoshida M, Nosaka K, Yasunaga J, Nishikata I, Morishita K, Matsuoka M. Aberrant expression of the MEL1S gene identified in association with hypomethylation in adult T-cell leukemia cells. Blood. 2004;103:2753-2760.
38. Arnulf B, Villemain A, Nicot C, et al. Human T-cell lymphotropic virus oncoprotein Tax represses TGF-beta 1 signaling in human T cells via c-Jun activation: a potential mechanism of HTLV-I leukemogenesis. Blood. 2002;100:4129-4138.
39. Xu X, Heidenreich O, Kitajima I, et al. Constitutively activated JNK is associated with HTLV-1 mediated tumorigenesis. Oncogene. 1996;13:135-142.
40. Postigo AA. Opposing functions of ZEB proteins in the regulation of the TGFβ/BMP signaling pathway. EMBO J. 2003;22:2443-2452.
41. Postigo AA, Depp JL, Taylor JJ, Kroll KL. Regulation of Smad signaling through a differential recruitment of coactivators and corepressors by ZEB proteins. EMBO J. 2003;22:2453-2462.
42. Peinado H, Olmeda D, Cano A. Snail, Zeb and bHLH factors in tumour progression: an alliance against the epithelial phenotype? Nat Rev Cancer. 2007;7:415-428.
43. Murakami Y. Involvement of a cell adhesion molecule, TSLC1/IGSF4, in human oncogenesis. Cancer Sci. 2005;96:543-552.
44. Yang L, Han Y, Saurez Saiz F, Minden MD. A tumor suppressor and oncogene: the WT1 story. Leukemia. 2007;21:868-876.
45. Dik WA, Pike-Overzet K, Weerkamp F, et al. New insights on human T cell development by quantitative T cell receptor gene rearrangement studies and gene expression profiling. J Exp Med. 2005;201:1715-1723.
46. Christ M, McCartney-Francis NL, Kulkarni AB, et al. Immune dysregulation in TGF-β1-deficient mice. J Immunol. 1994;153:1936-1946.
47. Plum J, De Smedt M, Leclercq G, Vandekerckhove B. Influence of TGF-β on murine thymocyte development in fetal thymus organ culture. J Immunol. 1995;154:5789-5798.
48. Postigo AA, Dean DC. Independent repressor domains in ZEB regulate muscle and T-cell differentiation. Mol Cell Biol. 1999;19:7961-7971.
49. Fontemaggi G, Gurtner A, Damalas A, et al. δEF1 repressor controls selectively p53 family members during differentiation. Oncogene. 2005;24:7273-7280.
50. Chen J, Yusuf I, Andersen HM, Fruman DA. FOXO transcription factors cooperate with δEF1 to activate growth suppressive genes in B lymphocytes. J Immunol. 2006;176:2711-2721.
51. Fukuda R, Hayashi A, Utsunomiya A, et al. Alteration of phosphatidylinositol 3-kinase cascade in the multilobulated nuclear formation of adult T cell leukemia/lymphoma (ATLL). Proc Natl Acad Sci U S A. 2005;102:15213-15218.

De novo CD5+ diffuse large B-cell lymphoma: results of a detailed clinicopathological review in 120 patients

Motoko Yamaguchi,[1] Naoya Nakamura,[2] Ritsuro Suzuki,[3] Yoshitoyo Kagami,[4] Masataka Okamoto,[5] Ryo Ichinohasama,[6] Tadashi Yoshino,[7] Junji Suzumiya,[8] Takuhei Murase,[9] Ikuo Miura,[10] Koichi Ohshima,[11] Momoko Nishikori,[12] Jun-ichi Tamaru,[13] Masafumi Taniwaki,[14] Masami Hirano,[5,15] Yasuo Morishima,[4] Ryuzo Ueda,[16] Hiroshi Shiku,[1] and Shigeo Nakamura[1]

[1]Mie University Graduate School of Medicine, Tsu; [2]Tokai University, Isehara; [3]Nagoya University Graduate School of Medicine, Nagoya; [4]Aichi Cancer Center, Nagoya; [5]Fujita Health University School of Medicine, Toyoake; [6]Tohoku University Postgraduate School of Medicine, Sendai; [7]Okayama University Graduate School of Medicine and Dentistry, Okayama; [8]Fukuoka University Chikushi Hospital, Fukuoka; [9]Nishio Municipal Hospital, Nishio; [10]St. Marianna Medical University, Kawasaki; [11]Kurume University School of Medicine, Kurume; [12]Kyoto University, Kyoto; [13]Saitama Medical Center, Kawagoe; [14]Kyoto Prefectural University of Medicine, Kyoto; [15]Meijo University, Nagoya, and [16]Nagoya City University Medical School, Nagoya, Japan

Acknowledgments: we thank the collaborators from the institutions for providing patients' data and specimens. A list of participating institutes is given in the Appendix. This paper was presented in part at the 49th Annual Meeting of the American Society of Hematology, Atlanta, December 2007.

Funding: this work was supported in part by Grants-in-Aid for Cancer Research (15-11, 19-8) from the Ministry of Health, Labour and Welfare, Japan.

Manuscript received January 24, 2008. Revised version arrived on March 26, 2008. Manuscript accepted April 15, 2008.

Correspondence:
Motoko Yamaguchi, M.D., Ph.D., Department of Hematology and Oncology, Mie University Graduate School of Medicine, 2-174 Edobashi, Tsu, Mie 514-8507, Japan.
E-mail: waniwani@clin.medic.mie-u.ac.jp

ABSTRACT

Background
De novo CD5-positive diffuse large B-cell lymphoma (CD5+ DLBCL) is clinicopathologically and genetically distinct from CD5-negative (CD5-) DLBCL and mantle cell lymphoma. The aim of this retrospective study was to clarify the histopathological spectrum and obtain new information on the therapeutic implications of CD5+ DLBCL.

Design and Methods
From 1984 to 2002, 120 patients with CD5+ DLBCL were selected from 13 collaborating institutes. We analyzed the relationship between their morphological features and long-term survival. The current series includes 101 patients described in our previous study.

Results
Four morphological variants were identified: common monomorphic n=91, giant cell-rich n=13, polymorphic n=14, and immunoblastic n=2. Intravascular or sinusoidal infiltration was seen in 38% of the cases. BCL2 protein expression in CD5+ DLBCL was more frequent than in CD5- DLBCL (p=0.0003). Immunohistochemical analysis in 44 consecutive cases of CD5+ DLBCL revealed that 82% of these cases 36/44 were non-germinal center B-cell type DLBCL. The 5-year overall survival rate of the patients with CD5+ DLBCL was 38% after a median observation time of 81 months. Patients with the common variant showed a better prognosis than those with the other three variants (p=0.011), and this was confirmed on multivariate analysis. Overall, 16 patients 13% developed central nervous system recurrence.

Conclusions
Our study revealed the morphological spectrum of CD5+ DLBCL, found that the incidence of central nervous system recurrence in this form of lymphoma in high, confirmed that CD5+ DLBCL frequently expresses BCL2 protein and showed that it is mainly included in the non-germinal center B-cell type of DLBCL.

Key words: diffuse large B-cell lymphoma, CD5, histopathology, BCL2, central nervous system.

Citation: Yamaguchi M, Nakamura N, Suzuki R, Kagami Y, Okamoto M, Ichinohasama R, Yoshino T, Suzumiya J, Murase T, Miura I, Ohshima K, Nishikori M, Tamaru J, Taniwaki M, Hirano M, Morishima Y, Ueda R, Shiku H and Nakamura S. De novo CD5+ diffuse large B-cell lymphoma: results of a detailed clinicopathological review in 120 patients. Haematologica 2008; 93:1195-1202. doi: 10.3324/haematol.12810

Introduction

Diffuse large B-cell lymphoma DLBCL constitutes the largest category of aggressive lymphomas, and is considered to have heterogeneous biological properties.[1,2] The phenomenon of CD5 expression in DLBCL evolving *de novo*, and not as a result of the transformation of chronic lymphocytic leukemia and mantle cell lymphoma, was first described by Matolcsy *et al.* in 1995.[3] Since then, accumulating clinicopathological evidence has gradually clarified that *de novo* CD5-positive ($CD5^+$) DLBCL constitutes a unique subgroup of DLBCL.[4-15] *De novo* $CD5^-$ DLBCL is associated with onset in old age, female predominance, advanced stage at diagnosis, the presence of B symptoms, high levels of lactate dehydrogenase, and the frequent involvement of extranodal sites. The genetic analysis of this lymphoma has suggested that it may originate from somatically mutated $CD5^-$ progenitor B cells.[5,6,8,13] Moreover, an analysis using cDNA microarray and comparative genomic hybridization technology demonstrated that *de novo* $CD5^+$ DLBCL is distinct from $CD5^-$ DLBCL and mantle cell lymphoma.[12,14-17] Cytogenetic analysis identified a subgroup of patients with *de novo* $CD5^+$ DLBCL with chromosomal abnormalities in 8p21 or 11q13 who have a poor prognosis.[18]

We reported that *de novo* $CD5^+$ DLBCL tumors usually show a centroblastic morphology, and 19% show an intravascular or sinusoidal growth pattern.[11] However, CD5 is expressed in some cases of intravascular large B-cell lymphoma[19-21] and T-cell-rich B-cell lymphoma,[22] and cases of $CD5^+$ follicular lymphoma[24,25] and $CD5^+$ Burkitt's lymphoma[26] have been reported. The relationship between these tumors and *de novo* $CD5^+$ DLBCL remains to be clarified. We reported that *de novo* $CD5^+$ DLBCL shows an aggressive clinical course, with a 5-year overall survival rate of 34%.[11] However, the median observation period in our previous study was 33 months; the results should, therefore, be confirmed by long-term survival analysis.

To clarify the histopathological spectrum of $CD5^+$ DLBCL and obtain new information on the therapeutic implications, we performed a detailed clinicopathological review and long-term follow-up analysis in a larger number of patients with *de novo* $CD5^+$ DLBCL.

Design and Methods

Patients

We selected 120 patients with *de novo* $CD5^+$ DLBCL from 13 collaborating institutes. All patients were diagnosed between 1984 and 2002 as having DLBCL according to the WHO classification,[2] and they had no past history of any other lymphoproliferative disorders. All specimens for histological and immunophenotypic studies were obtained at the initial presentation of the patients, and were examined for CD5 antigen expression by means of flow cytometry and/or immunohistochemistry. All patients were immunohistochemically confirmed to be cyclin D1-negative. The current series includes 101 of 109 *de novo* $CD5^+$ DLBCL cases described in our previous study.[11] Seven patients who fulfilled the diagnostic criteria for intravascular large B-cell lymphoma[2] and one patient with follicular colonization were excluded. The study was approved by the Ethics Committee of Mie University Graduate School of Medicine, and complied with the Helsinki Declaration.

Clinical information was obtained from the hospital records or supplied by the physicians at the collaborating centers.

Morphological evaluation

Tissue was fixed in 10% formalin and embedded in paraffin. Sections (5 μm thick) were stained with hematoxylin and eosin. We examined all the 120 initial diagnostic specimens of the *de novo* $CD5^+$ DLBCL cases, consisting of 85 lymphatic tissues such as lymph node, Waldeyer's ring, and spleen and 35 extranodal tissues with lymphomatous involvement. All cases were blindly reviewed twice by three of the authors (*MY, NN, and SN*). If discrepancies occurred, we discussed the cases while using a multiheaded microscope to reach a consensus.

Immunophenotypic study

Immunohistochemical and flow-cytometric analyses were performed as described previously.[27,28] The monoclonal antibodies used were Leu4 CD3, Leu1 CD5, and CALLA (CD10) (Becton Dickinson, Mountain View, CA, USA); J5 (CD10) and B1 (CD20) (Coulter, Hialeah, FL, USA); H107 (CD23) (Nichirei, Tokyo, Japan); MHM6 CD23, BerH2 CD30, UCHL1 CD45RO, HM57 CD79a, anti-immunoglobulin IgG, anti-IgA, anti-IgM, anti-IgD, anti-kappa, and anti-lambda (DAKO, Carpentaria, CA, USA); 4C7 (CD5) and NCL-CD10 CD10 Novocastra, Newcastle, UK, and cyclin D1 IBL, Gunma, Japan. Mor e than 20% positivity of the tumor cells was considered to indicate positivity for the purposes of this study. Based on preliminary data that the incidence of CD5 positivity in DLBCL examined with paraffin material is approximately half of that examined using frozen sections, and that it can be increased using more sensitive immunohistochemical methods (*Yamaguchi M et al., presented at the Annual Meeting of the Japanese Society of Lymphoreticular Tissue Research, 2000*), CD5 expression was examined primarily by flow cytometry and/or immunohistochemistry in the frozen sections from 104 cases of *de novo* $CD5^+$ DLBCL. In the remaining 16 cases, CD5 expression was examined immunohistochemically using paraffin-embedded sections. In fact, 75% or more of the neoplastic cells were confirmed to be positive for CD5 in the cases examined using paraffin-embedded material alone.

BCL2 protein expression was examined by means of immunohistochemistry using paraffin sections and a monoclonal antibody (BCL2, DAKO). Paraffin-embedded material for this study was available in 96 out of 120 cases. Staining for BCL2 was performed at the Aichi Cancer Center, and the data were compared with those for 150 cases of $CD5^-$ DLBCL, which were sequentially diagnosed at the Aichi Cancer Center during the same period as the *de novo* $CD5^+$ DLBCL cases. The reaction